Damping formulations for finite difference linear dynamic analyses: performance and practical recommendations

POST-PRINT VERSION, published in Computer and Geotechnics, 142 (2022) 104568, https://doi.org/10.1016/j.compgeo.2021.104568

Luca VERRUCCI *,[1], Alessandro PAGLIAROLI **, Giuseppe LANZO*, Francesco DI BUCCIO**, Alessandro Pio BIASCO***, Chiara CUCCI***

** Dipartimento di Ingegneria Strutturale e Geotecnica, Sapienza Università di Roma, Roma*

*** Dipartimento di Ingegneria e Geologia, Università degli Studi "G.d'Annunzio" Chieti-Pescara, Pescara*

**** PROGER S.p.A., Pescara*

Abstract

An in-depth study is presented on some numerical formulations used to reproduce damping of motion in solid continua. The focus is addressed in particular to those formulations that in the finite difference geotechnical code FLAC can be exploited to perform linear analyses. The numerical investigations are performed through a simple 1D model of a homogeneous soil deposit interested by a shear wave motion coming from the bedrock, and a gravity dam model subjected to seismic excitations in presence of dam-water-foundation interaction. The Rayleigh damping method is tested in particular to find an appropriate choice of the control frequency in order to minimize the problems of high-frequency overdamping. The analyses also investigate two other formulations (the local damping and its variant, the combined damping) that present the major advantages in providing a frequency independent action

[1] Corresponding Author, luca.verrucci@uniroma1.it

and in needing not significant computational resources. Limits and principal drawbacks of their possible use are highlighted.

Keywords:

CRITICAL DAMPING RATIO; RAYLEIGH DAMPING; LOCAL DAMPING; DYNAMIC ANALYSES; FINITE DIFFERENCE METHOD.

List of symbols

$[C]$	viscous damping matrix of a multiple degree of freedom system
$[K]$	stiffness matrix of a multiple degree of freedom system
$[M]$	mass matrix of a multiple degree of freedom system
A	displacement amplitude of a single degree of freedom system
c_m	viscous coefficient for a node of FLAC with mass proportional damping
D	material critical damping ratio
F	resultant force
F_d	damping force
f^*	frequency used in a single control frequency approach to the Rayleigh damping formulation
f_0	first natural (fundamental) frequency of a soil deposit
f_m	mean frequency of the input motion as in Rathje *et al.* (1998)
f_{min}	frequency at the minimum modal damping in the Rayleigh formulation
f_p	predominant frequency of an earthquake motion
f_t	tensile strength of the concrete
G	shear stiffness modulus
H	thickness of a soil deposit
K	bulk elastic modulus
k	stiffness of a single degree of freedom system
m	mass
T	period
$\dot{u}_i^{(t)}$	component i (i =x,y) of the velocity of a node of FLAC at time t
$u_i^{(t)}$	component i (i°=x,y) of the displacement of a node of FLAC at time t
v_0	initial velocity
V_S	shear wave velocity
W_E	maximum elastic energy accumulated

α	coefficient of the local damping formulation
α_R	mass proportional damping coefficient of the Rayleigh formulation
β_R	stiffness proportional damping coefficient of the Rayleigh formulation
γ	unit weight
Δt	timestep length in FLAC calculation
Δw	energy dissipated during each quarter of a cycle
ΔW	energy dissipated during the whole cycle
$\Delta\sigma_{ij,v}$	increment of stress of a single zone of FLAC with stiffness proportional damping
ξ^*, D^*	target critical damping ratio that is to be modelled
ξ_j	critical damping ratio for vibrational mode j of a multiple degree of freedom system
σ_{ij}	stress tensor of a single zone in FLAC
ω^*	circular frequency used in a single control frequency approach to the Rayleigh damping formulation
ω_0	first natural circular frequency of a soil deposit or natural frequency of a single degree of freedom system
ω_α	modified circular frequency of a single degree of freedom system damped through the local formulation
ω_j	circular frequency for vibrational mode j of a multiple degree of freedom system
ω_m, ω_n	frequencies used in a two control frequencies approach to the Rayleigh damping formulation

1. Introduction

The energy dissipation in soils and rocks is related to inner friction phenomena and to the hysteretic behavior under cyclic loading. In time-domain site response analyses it could be ideally represented by an appropriate nonlinear constitutive model. However, these models tend to be complex, embodying many material parameters, expensive to be calibrated in practice. At small to medium strain levels is usual to simulate the behavior of the materials through a linear constitutive model (with an appropriate choice of the stiffness) associated to an additional damping formulation.

Differently, if medium to large strain levels are attained, simple elasto-plastic (e.g. Mohr-Coulomb) or hyperbolic models (Hashash and Park, 2001; Matasovic, 2006) can be used,

that provide no energy loss at very small strains and therefore require an amount of damping to be added in the analyses.

The additional damping can be introduced in time-domain dynamic analyses in different ways, but the most used is the viscous Rayleigh Damping, hereafter RD (Chopra, 2007; Lanzo *et al.*, 2003; Park and Hashash, 2004). This approach can be easily implemented in finite elements and finite difference analyses.

Attention here is focused on the 2D finite difference FLAC code (Cundall, 2006; Itasca, 2011). The additional damping can be added in the FLAC analyses through the classic viscous Rayleigh Damping, or the alternative formulations named Local Damping, hereafter LD, and its variant, the Combined Damping, hereafter CD (Itasca, 2011). All these are *built-in* formulations. A further numerical technique was recently advanced, using a combination of one or more Maxwell components in parallel to the material stiffness, with a preliminary application to the 3D version of the code (Dawson & Cheng, 2021).

The use of RD, common in time domain analyses, is characterized by two major drawbacks: a rate-dependent damping (conversely to what is experimentally observed for soils in the frequency range excited by earthquakes) and a severe reduction in the timestep length (therefore a severe increment of time running) for explicit codes. On the contrary, LD and CD formulations are frequency independent, and they do not significantly affect the runtime; however, the use of LD and CD is only partially documented in the literature and there is evidence to suggest that, for irregular waveforms, local damping underdamps the high frequency components and may introduce high frequency noises (Itasca, 2011; Manica *et al.*, 2014).

The aim of the paper is to gain insight into the different damping formulations that are implemented in the FLAC code, focusing on Rayleigh, Local and Combined Damping formulations when they are applied to linear analyses. Parametric linear analyses were first conducted on an ideal soil profile excited by several accelerograms with different frequency

content. A real case is then addressed, i.e. the seismic analysis of a concrete gravity dam, modelled through FLAC taking into consideration simultaneously the dam-water-foundation interaction. A linear model has been adopted for the dam body using RD, LD and CD formulations to model all the amount of material damping; this choice allowed to better highlight the differences between the three formulations.

Some practical recommendations are finally provided for FLAC users, in particular: i) criteria for selecting control frequencies and target damping in Rayleigh damping formulation. ii) advantages and drawbacks of RD, LD and CD formulations and suggestions for selecting the appropriate choice of additional damping by balancing accuracy and speed of the analysis.

2. Damping models in FLAC

2.1. Introduction

A brief recall of the numerical background of the stress-strain analysis through the finite difference method is needed to understand the differences in damping formulations. The FLAC code solves the dynamic equilibrium equations of a continuous medium by dividing the 2D space into a mesh of quadrilateral zones with nodes at the vertexes (Itasca, 2011). Each zone is composed by two overlaid pairs of adjacent constant-strain triangular elements. For each node a pertaining area can be outlined as the sum of portions of the triangular elements converging to it.

At a generic time t of the analysis the resultant out-of-balance force vector $F^{(t)}$ on each node is calculated through integration of both the body force field and the stress tensor gradient over the area pertaining to the node; for nodes on the boundaries also possible surface forces contribute to $F^{(t)}$.

Each node will be accelerated according to the explicit finite difference form of Newton's second law of motion, that has the following form for each component (in the 2D formulation *i*=*x*,*y*):

$$\dot{u}_i^{\left(t+\frac{\Delta t}{2}\right)} = \dot{u}_i^{\left(t-\frac{\Delta t}{2}\right)} + F_i^{(t)} \frac{\Delta t}{m} \qquad (1)$$

where $\dot{u}_i$ is the nodal velocity and the superscripts denote the time at which the corresponding variable is evaluated, m is the lumped mass pertaining to the node and Δt is the timestep length. Once the velocity has been updated for each node, the strain rates tensor of each triangular elements can be calculated through integrating the velocity flow across its perimeter. The constitutive model applied in each zone gives the new stress rate tensor. This requires an update of the previous nodal force balances and another cycle can be initiated.

2.2. Rayleigh Damping (RD)

The Rayleigh damping is a well-known formulation in modal analysis of structural systems and in the finite element method of continuum analysis (Chopra, 2007, Zienkiewicz *et al.*, 2005). In these fields the Rayleigh damping is generally expressed in matrix form as a linear combination of both mass [*M*] and stiffness [*K*] matrices (full Rayleigh formulation):

$$[C] = \alpha_R [M] + \beta_R [K] \qquad (2)$$

where [*C*] is the damping matrix, α_R and β_R are the mass and stiffness damping coefficients, respectively. In the finite difference framework, the mass proportional term is obtained through a viscous dashpot connecting every FLAC node to "ground" (i.e. to a fixed reference frame). The viscous coefficients of dashpots are $c_m = \alpha \cdot m$, being m the mass lumped to the node. The node force balance (1) will be so changed in:

$$\dot{u}_i^{\left(t+\frac{\Delta t}{2}\right)} = \dot{u}_i^{\left(t-\frac{\Delta t}{2}\right)} + \left[F_i^{(t)} - c_m \dot{u}_i^{(t-\frac{\Delta t}{2})}\right]\frac{\Delta t}{m} \qquad (3)$$

The stiffness proportional term of the Rayleigh Damping is not directly calculated as a further force acting on the node. Just after the new stress tensor $\sigma_{ij,new}$ is computed through invoking the constitutive model of each zone at the end of each timestep, a further viscous stress increment $\Delta\sigma_{ij,v}$ is added:

$$\Delta\sigma_{ij,v} = \frac{\beta_R}{\Delta t}\left(\sigma_{ij,new} - \sigma_{ij,o}\right) \qquad (4)$$

where $\sigma_{ij,o}$ is the original value of the stress tensor, prior to invoking the constitutive relationship. The viscous stress increment for each zone concurring to the single node is taken into account in the successive nodal force balance to compute $F^{(t)}$ but it is not accumulated to the current stress state of the zone.

Bathe and Wilson (1976) showed that this formulation provides a different critical damping ratio ξ_j for each vibrational mode of a continuous system:

$$\xi_j = \frac{1}{2}\left(\frac{\alpha_R}{\omega_j} + \beta_R \omega_j\right) \qquad (5)$$

where ω_j is the circular frequency for mode j. Therefore, if a material with a certain "target" damping ratio ξ^* is to be simulated (generally the soil damping ratio D), determination of the proper α_R and β_R coefficients can follows two approaches. The first approach uses a single control frequency ω^* that could represent the main frequency of interest for the system. Assuming that the material damping ratio is equally divided between the mass-proportional component and the stiffness-proportional one, from Equation (5) follows that:

$$\alpha_R = \xi^* \omega^* \qquad \beta_R = \xi^* / \omega^* \qquad (6)$$

Hence the modal damping ratio ξ_j can be rewritten:

$$\xi_j = \frac{\xi^*}{2}\left(\frac{\omega^*}{\omega_j} + \frac{\omega_j}{\omega^*}\right) \qquad (7)$$

The relation between ξ_j and ω_j is presented in Figure 1a with a bold line. This figure shows that ξ_j attains its minimum value ξ^* at the control frequency ω^* while all other frequencies are more heavily damped. In site response analyses it is often assumed that ω^* is equal to the first natural circular frequency of soil deposit ω_0.

In the two control frequencies approach, if the target damping ratio is attained at the two modes m and n with circular frequencies ω_m and ω_n (i.e. $\xi_m = \xi_n = \xi^*$), the expressions for α_R and β_R are:

$$\alpha_R = \xi^* \frac{2\omega_m \omega_n}{\omega_m + \omega_n} \qquad \beta_R = \xi^* \frac{2}{\omega_m + \omega_n} \qquad (8)$$

and the modal damping ratio ξ_j for the j_{th} mode is given by:

$$\xi_j = \frac{\xi^*}{\omega_{m+}\omega_n} \left(\frac{\omega_m \omega_n}{\omega_j} + \omega_j \right) \qquad (9)$$

The relationship between modal damping ratio ξ_j and natural frequency ω_j is shown in Figure 1b. It is observed that for the frequencies between ω_m and ω_n, damping ratio is slightly less than ξ^* while for frequencies outside of this range larger damping ratios are obtained. The appropriate selection of modes m and n for which the specified damping ratio value ξ^* is assumed should guarantee reasonable constant damping in all the modes contributing significantly to the response (Kwok *et al.*, 2007). In site response analyses, one control frequency is usually set at ω_0 while the second one is a multiple of ω_0. As an example, in QUAD4M the two control frequencies are automatically fixed by the code such that the first one is the fundamental frequency of the whole system ($\omega_1 = \omega_0$) while for the second one it is assumed $\omega_2 = n\ \omega_0$ with n being the smallest odd integer such that ω_2 exceeds the predominant frequency (ω_p) of the earthquake motion provided by the user (Lanzo *et al.*, 2003, 2004).

The same modal damping distribution associated to the two control frequencies ω_m and ω_n can be obtained through an equivalent single control frequency approach. In fact, once the coefficients α_R and β_R are calculated through Equations (8), Equations (6) allow to obtain the coordinate of the minimum of the distribution that are the equivalent parameters to be specified:

$$D_{min} = \sqrt{\alpha_R \beta_R}, \qquad \omega_{min} = \sqrt{\frac{\alpha_R}{\beta_R}} \qquad (10)$$

A last approach rarely used in dynamic analyses is the simplified Rayleigh formulation. It corresponds to the limit case of the Rayleigh damping formulation with α_R=0 in Equation (2) (i.e., only stiffness-proportional damping). In this case the coefficient β_R is given by:

$$\beta_R = 2\xi^* / \omega^* \qquad (11)$$

while the modal damping ratio ξ_j linearly increases with frequency according to:

$$\xi_j = (\xi^* / \omega^*)\, \omega_j \qquad (12)$$

as shown in Figure 1c. The damping ratio is therefore highly overestimated for frequency higher than ω^*. Generally, in the practice it is suggested to set $\omega^* = \omega_0$ and ξ^* =D.

The nonlinear finite difference FLAC code uses the full Rayleigh formulation with a single control frequency. To obtain reliable results it is necessary to choose suitable values for the target damping ratio ξ^* and the control frequency ω^*.

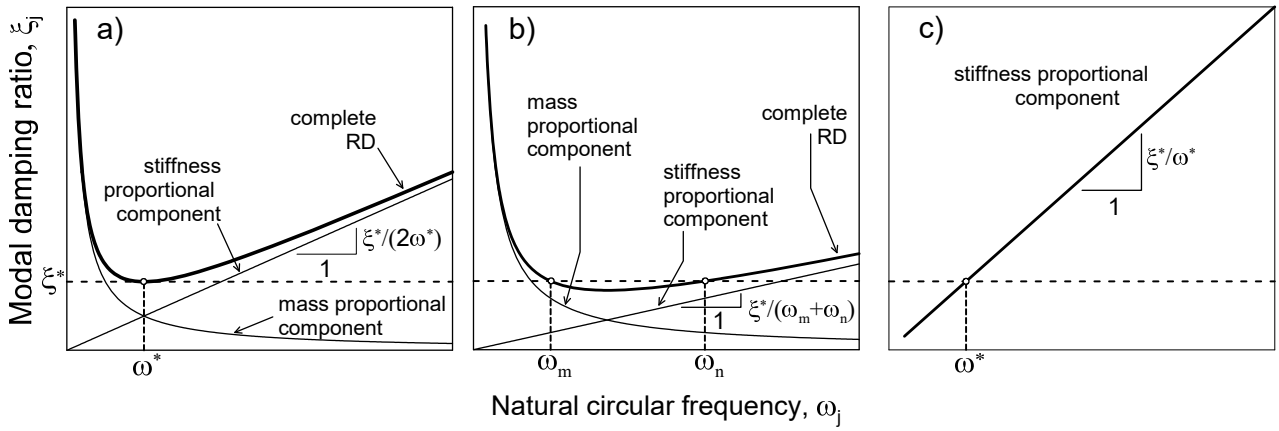

Figure 1. Full Rayleigh damping formulations with (a) single control frequency and (b) two control frequencies; Simplified Rayleigh damping formulation (c).

2.3. Local Damping (LD)

To overcome the problems associated to the Rayleigh damping, a form of damping called non-viscous local damping has been implemented in FLAC. It was originally designed to provide a numerical damping to the motion that is generated by the dynamic formulation of the solution in static or quasi-static simulations.

In this condition Equation (3) is replaced by the following equation:

$$\dot{u}_i^{\left(t+\frac{\Delta t}{2}\right)} = \dot{u}_i^{\left(t-\frac{\Delta t}{2}\right)} + \left[F_i^{(t)} + (F_d)_i\right]\frac{\Delta t}{m} \qquad (13)$$

where

$$(F_d)_i = -\alpha \left|F_i^{(t)}\right| \; sgn\left(\dot{u}_i^{\left(t-\frac{\Delta t}{2}\right)}\right) \qquad (14)$$

is the damping force component, α is a constant, *sgn* is the sign function. It is evident immediately from Eqs. (13) and (14) that the damping force on a node has a magnitude proportional to the size of the unbalanced force and a direction such that energy is always dissipated (i.e. opposite to the current velocity component). With these features the formulation of the LD can be considered equivalent to apply the original resultant force F_i to the gridpoint *i* having a mass modified following the factor $(1\pm\alpha)^{-1}$, the sign depending on the velocity versus (see Appendix A).

The amount of damping is controlled by the coefficient α which is related to the soil damping ratio *D* by the following equation (Itasca, 2011):

$$\alpha = \pi D \qquad (15)$$

A theoretical framework on the source of this expression is provided in Appendix A. The use of local damping is obviously simpler than Rayleigh damping, because it is rate (i.e. frequency) independent and needs no estimate of the natural frequency of the modelled system.

However, from Equation (14) it is apparent that the nodal damping force can change its sign (depending on the velocity sign) also having a finite, not null, modulus (depending on the out-of-balance force modulus), thus imposing a discontinuity in the node acceleration histories. As a consequence, a high frequency "noise" is introduced in the acceleration time histories and the high frequency damping is not well simulated (Itasca, 2011; Liu *et al.*, 2014; Manica *et al.*, 2014).

The effectiveness of the LD formulation for damping stress-strain waves in the continuum is strictly linked to the existence of zero-crossing instants in the time histories of the velocity components. If the velocity components of the nodes oscillate without sign changing the effect of Equation (14) is only to consider the lumped masses of nodes permanently augmented (or diminished) by a fraction. In other words, the “local” character of LD cannot recognize oscillating strains of a region when the whole region is involved into a global uni-directional (even if not uniform) motion. This case can be easily encountered for example in presence of a plastic flow but also when, in a multiple degrees of freedom system, the motion associated to a high frequency is overlaid to the motion of a low frequency harmonic with high amplitude. The high frequency harmonic can be hidden with respect to the local damping action and a high frequency overestimation results.

2.4. Combined Damping (CD)

In order to develop a more general damping formulation that works also in presence of global mass movements, sgn($\dot{F}$) can replace $-$sgn($\dot{u}$) in the damping force expressed by Equation (14), thus obtaining:

$$(F_d)_i = \alpha \left|F_i^{(t)}\right| \; sgn\left(\dot{F}_i^{\left(t-\frac{\Delta t}{2}\right)}\right) \quad (16)$$

For a single degree of freedom system this formulation is perfectly coincident to that of the LD (Equation (14)). In fact in this case the unbalanced force *F* corresponds to the elastic recall force *F = -ku,* whose sign is opposite to the displacement *u* sign. Therefore sign of $\dot{F}$ is opposite to $\dot{u}$ sign. In general, for systems with multiple degrees of freedom, the change of sign of $\dot{F}$ is equal to change of sign in the oscillating part of the velocity, independently from its mean value that can have permanent either positive or negative value. This damping force is independent of velocity and is therefore not as efficient as the local damping. In order to combine the advantages of both expressions of local damping, in FLAC a combination of both F_d formulas in equal proportions has been implemented:

$$(F_d)_i = -\alpha \left|F_i^{(t)}\right| \frac{\left(sgn\left(\dot{u}_i^{\left(t-\frac{\Delta t}{2}\right)}\right) - sgn\left(\dot{F}_i^{\left(t-\frac{\Delta t}{2}\right)}\right)\right)}{2} \quad (17)$$

and it is known as Combined Damping.

Despite the similar behavior in elementary systems, for multiple degrees of freedom systems the CD formulation has a further advantage respect to the LD. It allows to distribute the acceleration discontinuities over a higher number of time instants (i.e., when either velocity or unbalanced force rate change sign). Therefore Equation (17) entails a higher number of acceleration discontinuities, each one of a smaller amount with respect to Equation (14). A significant fading of the high frequency noise is therefore obtained.

Two final notes should be highlighted about the overestimation of the high frequencies for both the LD and CD formulations. 1) the amplification of the high frequencies motion is partially reduced in the velocity and the displacement time histories, whose integration is weakly affected by the acceleration discontinuities. 2) a significant fraction of the high frequency motion is constituted by a numerical fast vibration of the grid nodes, without a spatial coherency; therefore this part can be significantly reduced if the mean motion of a set of near nodes is considered rather than the motion of a single node.

In order to test the different damping formulations, the damped free vibration of a single square zone (side l=1 m long) of a visco-elastic material with density ρ=1600 kg/m^3 and shear modulus G=0.64 MPa (first mode frequency 4.5 Hz) was studied (Fig. 2). The zone is subjected to a single sinusoidal horizontal acceleration pulse at the bottom and the response at the higher side is recorded. The critical damping ratio has been set to 5% and the three damping formulations described above were employed (RD with control frequency 4.5 Hz, LD and CD). The horizontal acceleration and the Fourier amplitude are reported in Figure 2. Minor differences can be observed among the different damping schemes. A small amount of noise at selected frequencies (about 13.5 and 22.5 Hz) is introduced by Local and Combined Damping thus resulting in a small overestimation of peak response in time domain.

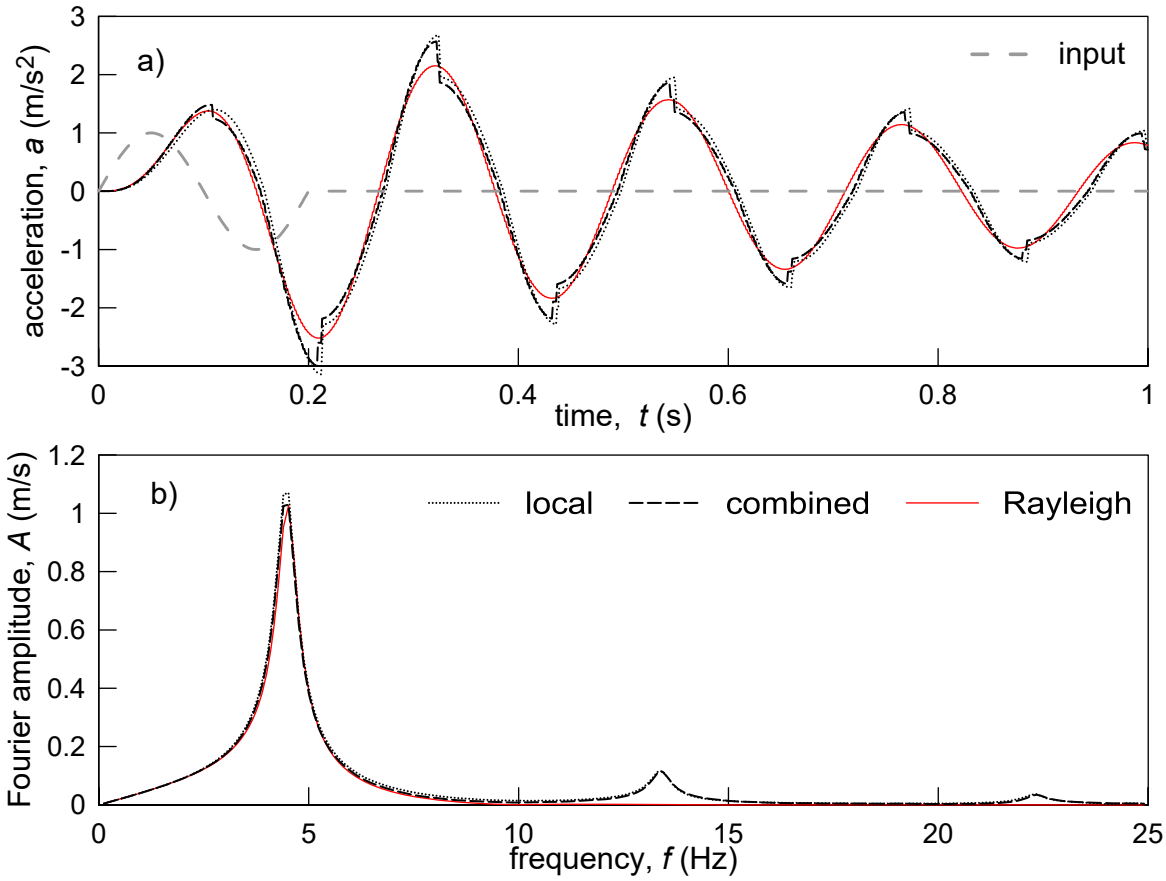

Figure 2. Dynamic response of a single zone to a sinusoidal pulse adopting the different FLAC damping formulations. Time domain response of acceleration (a) and amplitude Fourier spectra (b)

3. Parametric study on a virtual soil deposits

3.1. Introduction

To quantitatively evaluate the performance of the different damping formulations implemented in FLAC, parametric 1D linear visco-elastic analyses were initially performed on a homogeneous virtual soil deposits. A single soil layer with thickness H = 30 m, unit weight γ= 20 kN/m^3, shear wave velocity V_S=300 m/s and damping ratio D=5% has been first analyzed, thus resulting in a fundamental frequency f_0 =2.5 Hz (T_0=0.4 s). The analyses were then repeated on the same model using a shear wave velocity V_S = 100 m/s for the deposit, thus resulting in a fundamental frequency f_0 = 0.83 Hz (T_0 = 1.2 s). The underlying bedrock is characterized by γ = 22 kN/m^3 and V_S = 1000 m/s. A compliant (i.e. elastic) base scheme was adopted in the analyses by applying at the bottom of the mesh the input motion

in terms of shear stress time-histories (Joyner and Chen, 1975) coupled with Lysmer-Kuhlemeyer viscous boundary conditions (Lysmer and Kuhlemeyer, 1969). Six real accelerograms have been selected to cover a wide predominant frequency range, from 0.9 to 8.5 Hz (Tab.1) thus exciting different modes of vibration of the soil deposit. These signals were scaled to an outcropping PGA = 0.2*g*.

The purpose of these analyses was twofold: 1) to identify a strategy to select the target damping ratio *D* and the control frequency *f** in full Rayleigh formulation with single control frequency for FLAC analyses; 2) to evaluate the performance of FLAC Local/Combined damping formulations with respect to the "standard" Rayleigh damping. The seismic responses obtained by using a frequency domain code (thus implementing a frequency independent damping) has been assumed as reference. In particular, these reference analyses were carried out by the frequency-domain ProSHAKE code (EduPro Civil System, 1998), which applies a frequency-independent damping.

Table 1. Accelerograms employed for comparative analyses

#	station	component	earthquake, year	mean frequency f_m (Hz)	predominant frequency f_p (Hz)	Two-control equivalent freq. f_{min} (Hz)
1	Port Island	NS	Kobe 1994	0.68	0.91	2.5
2	Taft	S69E	Kern County 1952	1.87	2.27	2.5
3	Sturno	NS	Irpinia 1980	1.44	2.63	4.33
4	Gilroy2	90	Loma Prieta 1989	1.30	3.33	4.33
5	Gilroy2	50	Coyote Lake 1979	2.69	5.56	4.33
6	Tarcento	NS	Friuli 1976	2.70	8.33	5.59

3.2. Performance of single control frequency RD formulation

A first set of FLAC analyses has been carried out by setting the target damping ratio equal to the soil damping ratio (D^*=5%) and adopting four different strategies to fix the control frequency: f^* has been assumed in succession equal to the soil deposit fundamental frequency f_0, the predominant frequency f_p, the mean frequency f_m of the input motion (Rathje *et al.* 1998), and the f_{min}, corresponding to the approach equivalent to the two control frequencies formulation (computed according equations 10 and 8 with the two control

frequencies selected according to the QUAD4M procedure described at paragraph 2.2). In this latter approach D^* has been set to D_{min} computed according to (10). The values of the values of control frequency f^* are reported in Table 1 while according to eq. (10) is D_{min}=5% for input #1-#2, 4.33% for input #-3-#5 and 3.73% for input #6.

The results of the parametric FLAC analyses, for all selected input accelerograms, are compared with the reference results in terms of PGA profiles along depth and response spectra at soil surface, in Figures 3 and 4 respectively. No significant differences among the different strategies for setting f^* can be observed for the results obtained with input from #1 to #4 where the reference solution (Proshake) is satisfactorily matched both in terms of PGA profiles and response spectra at surface. Only a slight underestimation of high frequencies with respect to Proshake can be observed (Figure 4). Higher differences can be observed for input #5 (Gilroy 2-50) and #6 (Tarcento NS) where the reference solution is poorly approximated especially in the high frequency range (including the PGA profile). For these two inputs, characterized by $f_m > f_0$, slightly better approximation of the reference solution is achieved by setting $f^*=f_m$.

In order to quantitatively identify the most appropriate choice for f^*, i.e. the choice that minimizes the differences with respect to the reference solution, a synthetic parameter *RSS* (Residual Sum of Squares) has been introduced:

$$RSS = \sum_{i=1}^{n} \left(y_i - y_{ref,i}\right)^2 \qquad (18)$$

where y_i is the value of ground motion parameter (PGA or spectral acceleration) predicted with FLAC analysis and $y_{ref,i}$ is the reference value of the parameter computed using frequency-domain code while n is the total number of estimations (i.e., either the number of PGA values along the profile or the number of period values at which the response spectrum is defined). Obviously the lower the value of the *RSS* parameter the better the agreement of FLAC predictions with the reference results.

Table 2. RSS values computed for FLAC analyses to evaluate the performance of single control frequency Rayleigh formulation with respect to frequency independent solution. Minimum values are highlighted in bold text.

	control frequency	#1	#2	#3	#4	#5	#6
RSS from PGA Profile	f_0	0.0010	0.0023	**0.0083**	0.0036	0.0185	0.0777
	f_p	**0.0002**	0.0020	0.0096	**0.0033**	0.0553	0.0930
	f_m	0.0008	**0.0017**	0.0126	0.0072	**0.0176**	**0.0747**
	$f_{m\,/\,}D_{min}$	0.0010	0.0023	0.0165	0.0078	0.0283	0.1018
RSS from Response Spectra	f_0	**0.0251**	0.0497	**0.0853**	**0.0904**	0.1933	0.4545
	f_p	0.0306	**0.0460**	0.0894	0.1322	0.5195	1.3920
	f_m	0.0546	0.0488	0.1479	0.1643	**0.1881**	**0.4393**
	$f_{min\,/\,}D_{min}$	**0.0251**	0.0497	0.2653	0.2769	0.3978	1.3976

From *RSS* values reported in Tab. 2, two different scenarios can be outlined.

For input #1-#4 characterized by $f_m < f_0$ no appreciable influence of f^* selection is observed: f_0 or f_p generally provide the best performance but the performance of the different f^* is comparable as observed in Figures 3-4 previously discussed. On the contrary, for input #5-#6 ($f_m > f_0$), selecting $f^*=f_m$ seems the best choice to match the frequency independent reference solution, even if also f_0 provide satisfactory matching.

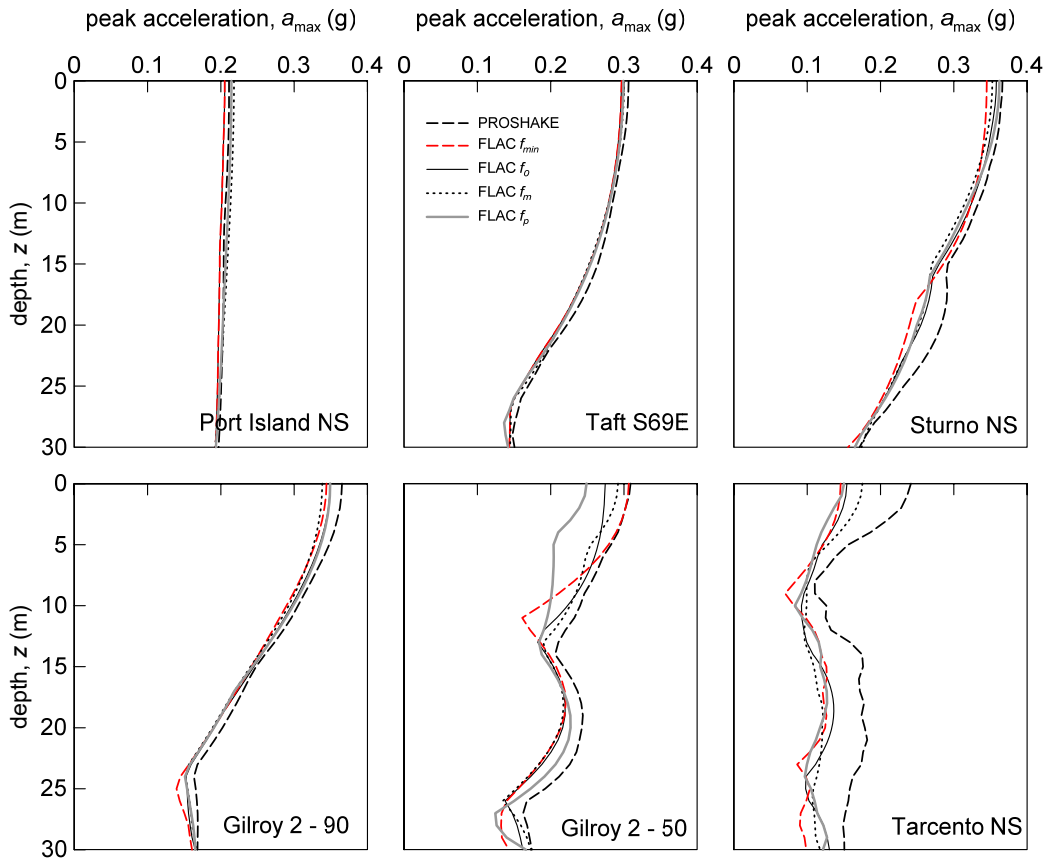

Figure 3. FLAC single control frequency Rayleigh formulation: comparison of PGA profiles for all selected input accelerograms (D* =5% and different strategies for setting the control frequency) – V_s=300 m/s homogeneous soil deposit (f_0=2.5 Hz)

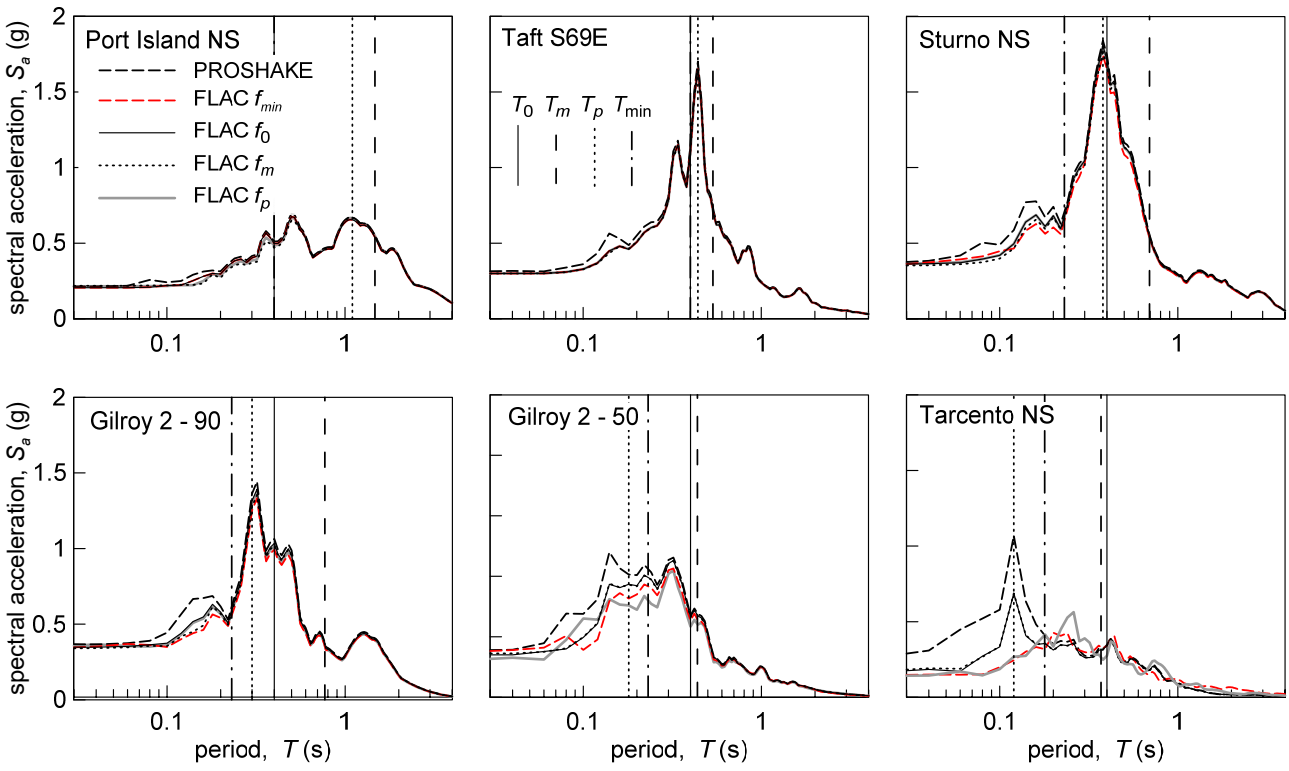

Figure 4. FLAC single control frequency Rayleigh formulation: comparison of response spectra at the surface of soil deposit for all selected input accelerograms (D* =5% and different strategies for setting the control frequency); fundamental,

minimum, mean and predominant frequencies (f_0, f_{min}, f_m and f_p) are highlighted in the plots – V_s=300 m/s homogeneous soil deposit (f_0=2.5 Hz)

In order to further explore these findings, additional analyses have been then carried out on the previous deposit in which V_s has been updated to 100 m/s. The deposit is now characterised by a fundamental frequency f_0 =0.83 Hz (T_0=1.2 s) and all the input accelerograms have $f_m > f_0$. The results of the parametric FLAC analyses, for all selected input accelerograms, are compared with the reference results in terms of PGA profiles along depth and response spectra at soil surface in Figures 5 and 6 respectively.

The analyses show that the results for input characterized by $f_m > f_0$ are highly sensitive on the value adopted for the control frequency. The choice of $f^*=f_0$ generally underestimates the ground motion both in time and frequency domains. This underestimation is particularly severe for motion characterized by predominant frequency well above f_0 or, in general, by a rich energy content at frequency higher than f_0 exciting the vibration mode higher than first (see for example Sturno NS, Gilroy 2-50, Tarcento NS inputs). Only for Port Island input, for which the response is essentially conditioned by the first mode of vibrating, all the curves coincide with the frequency independent response. A better performance has been obtained assuming a control frequency more representative of input motion as f_m or f_p. The comparison with ProSHAKE reference solution is very satisfactory for all selected inputs except for Tarcento high-frequency input motion. Finally the adoption of f_{min} and D_{min}, (i.e., approach equivalent to the full Rayleigh formulation with two control frequencies) provides results that are consistent with the results by frequency independent damping analyses for all selected input motions; the maximum differences between the two reference codes are generally lower than 10 % and 20 %, looking at the results expressed in time and frequency domains, respectively.

From *RSS* values reported in Tab. 3, the best performance in terms of PGA profiles and response spectra at surface is obtained for f_{min} - D_{min} strategy while f_m generally perform better than $f^*=f_p$ and $f^*=f_0$.

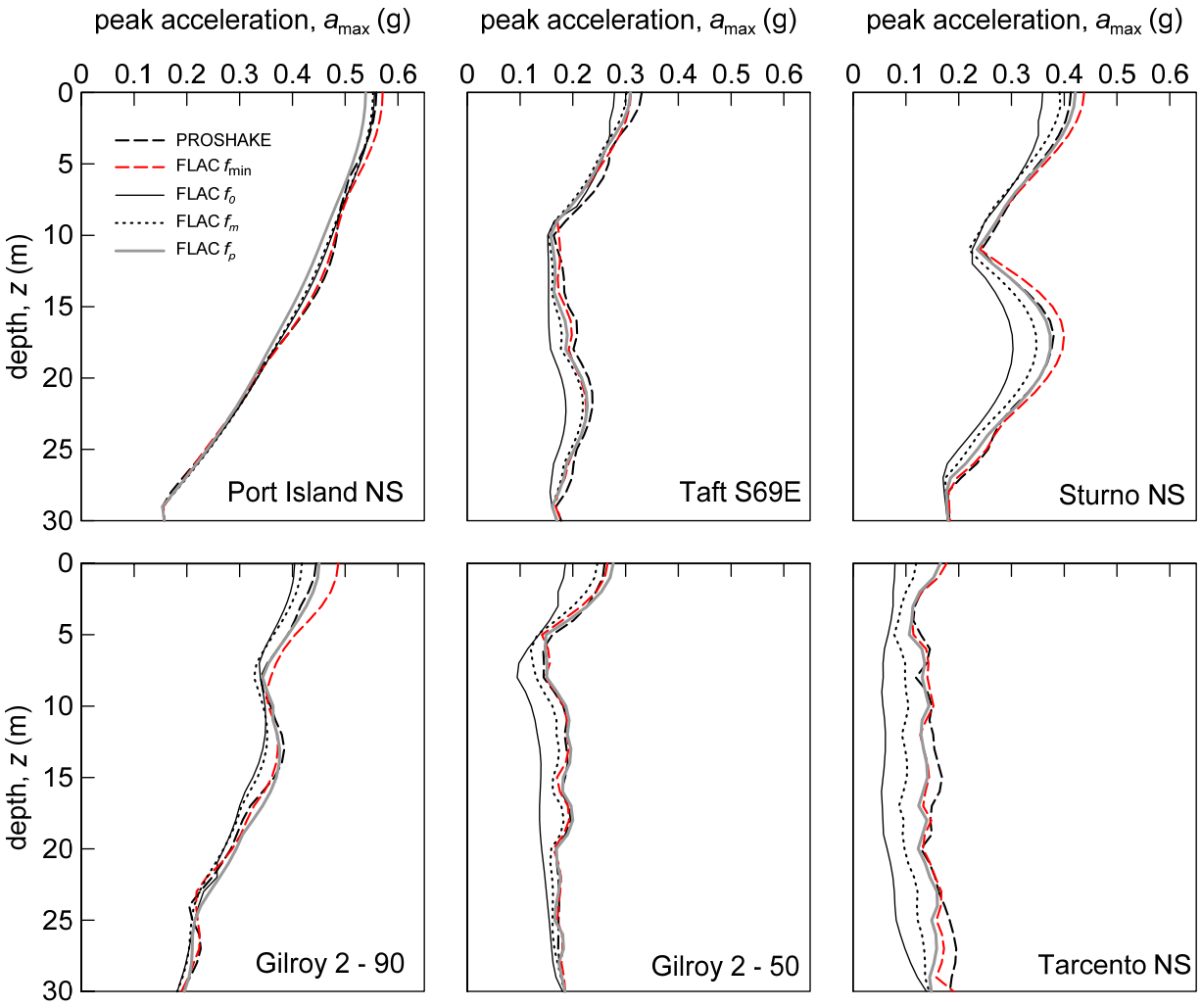

Figure 5. FLAC single control frequency Rayleigh formulation: comparison of PGA profiles for all selected input accelerograms (D^* =5% and different control frequencies) – V_s=100 m/s homogeneous soil deposit (f_0=0.83 Hz)

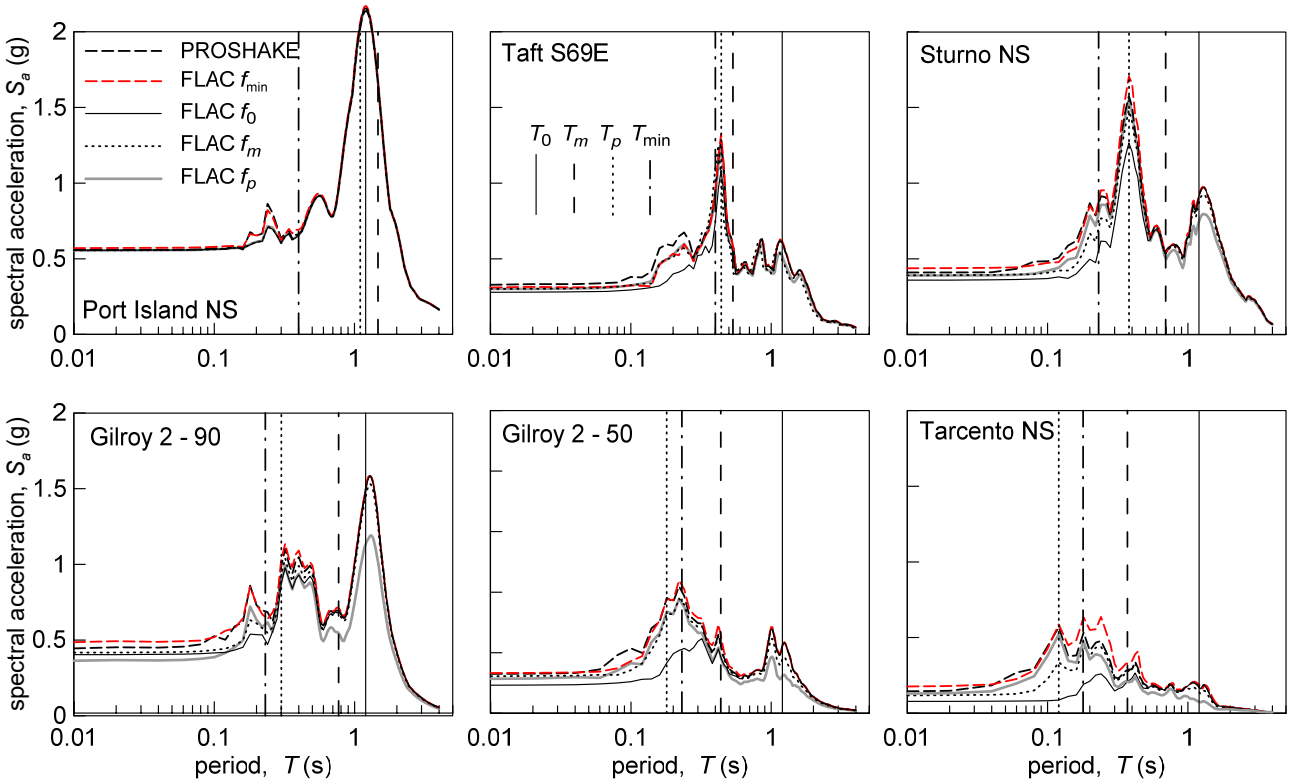

Figure 6. FLAC single control frequency Rayleigh formulation: comparison of response spectra at the surface of soil deposit for all selected input accelerograms (D^* =5% and different control frequencies); fundamental, mean and predominant frequencies (f_0, f_m and f_p) are highlighted in the plots – V_S=100 m/s homogeneous soil deposit (f_0=0.83 Hz)

Table 3. RSS values computed for FLAC analyses to evaluate the performance of single control frequency Rayleigh formulation with respect to frequency independent solution. Minimum values are highlighted in bold text.

		control frequency	#1	#2	#3	#4	#5	#6
RSS from PGA Profile	D^*=5%	f_0	0.0020	0.0391	0.0676	0.0185	0.0623	0.2167
		f_p	0.0019	0.0135	0.0188	0.1080	0.0115	0.0519
		f_m	**0.0002**	0.0134	0.0178	0.0126	0.0088	0.0747
	D_{min}	f_{min}	0.0015	**0.0046**	0.0064	0.0096	0.0018	**0.0076**
	D^* from Equation(19)	f_m	**0.0002**	0.0069	**0.0020**	**0.0037**	**0.0014**	0.0139
RSS from Response Spectra	D^*=5%	f_0	0.0636	0.5982	1.3150	0.4330	1.1308	0.9565
		f_p	0.0538	0.2177	0.8224	4.2299	1.0512	0.4024
		f_m	0.0598	0.6948	0.3568	0.2592	0.2685	0.2086
	D_{min}	f_{min}	**0.0439**	0.0753	0.1221	**0.0412**	**0.0447**	0.1602
	D^* from Equation(19)	f_m	0.0600	**0.0750**	**0.0993**	0.1030	0.0861	**0.0760**

In order to further improve the performance of the approach with $f^*=f_m$, a reduction of target damping value, D^* with respect to actual soil damping ratio, D can be considered. This should balance the overdamping observed with respect to reference solution (Figures 5 and 6).

The FLAC analyses were therefore repeated by setting $f^*=f_m$ and assuming a different target damping ratio D^* for each input motion, as computed through the following expressions:

$$D^* = \begin{cases} \dfrac{D}{f_1+f_2}\left(\dfrac{f_1 f_2}{f_m}+f_m\right) \Leftrightarrow f_m \in [f_1, f_2] \\ \\ D \Leftrightarrow f_m \notin [f_1, f_2] \end{cases} \qquad (19)$$

$$\begin{cases} f_1 = f_0 \\ f_2 = n f_1 \end{cases} \quad \text{with n closest odd integer greater than } \frac{f_p}{f_0}$$

In other words, the target damping ratio is forced to assume at the control frequency ($f^*=f_m$) the same value it would have at the same frequency in a two control frequencies approach (see Equation (9)). The resulting damping variation with frequency and a comparison with the two control frequencies approach is shown as an example in Figure 7 for input Gilroy2-90 which provided a target parameter D^*=3.97%. The target parameters for each input are shown in Table 4.

Table 4. Results from Equation (19)

Input accelerogram	f_m (Hz)	f_p (Hz)	f_0 (Hz)	f_1 (Hz)	f_2 (Hz)	D (%)	D^* (%)
#1	0.68	0.91	0.83	0.83	2.49	5.00	**5.00**
#2	1.87	2.27	0.83	0.83	2.49	5.00	**4.48**
#3	1.44	2.63	0.83	0.83	4.15	5.00	**3.85**
#4	1.30	3.33	0.83	0.83	4.15	5.00	**3.97**
#5	2.69	5.56	0.83	0.83	5.81	5.00	**3.38**
#6	2.70	8.33	0.83	0.83	9.13	5.00	**2.76**

The results of the FLAC analyses with $f^*=f_m$ and D^* evaluated according to the proposed expression in Equation (19) are compared with the reference results in terms of PGA profiles and response spectra at soil surface in Figures 8 and 9 respectively. In the same figures the results obtained with $f^*=f_m$ and D^*=5%, previously discussed, are also reported for comparison. As expected, a target damping ratio reduced with respect to the actual value of soil, significantly improve the prediction with respect to D^*=5% as confirmed also by the

lower values of *RSS* in Table 3. The single control frequency approach using the proposed values of D^* and $f^*=f_m$ lead to results comparable with those obtained with the f_{min} - D_{min} approach or even better: as matter of fact the RSS associated to D^*-f_m strategy are minimum for 4 and 3 cases (over 6) for PGA and response spectra, respectively (Table 3).

Equation (19) can be used for any soil profiles, also multi-layered, after the value of the fundamental frequency f_0 has been assessed. The f_0 assessment is straightforward for an uniform deposit, but for any other layout it can be found through the calculation of the transfer function of the ground motion with respect to the input motion.

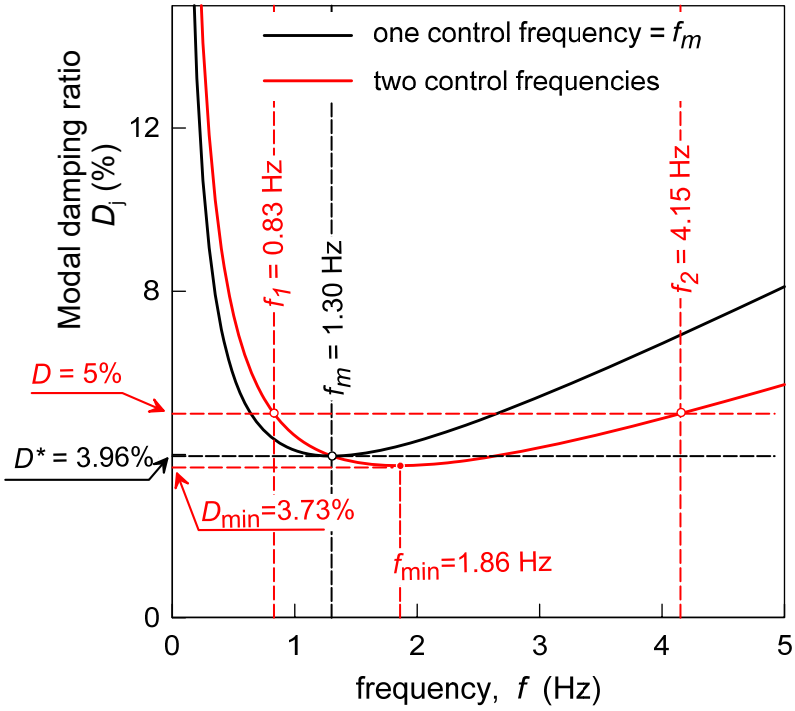

Figure 7. Proposed procedure for the definition of target damping ratio D* in single control frequency approach (input #4: Gilroy2-90)

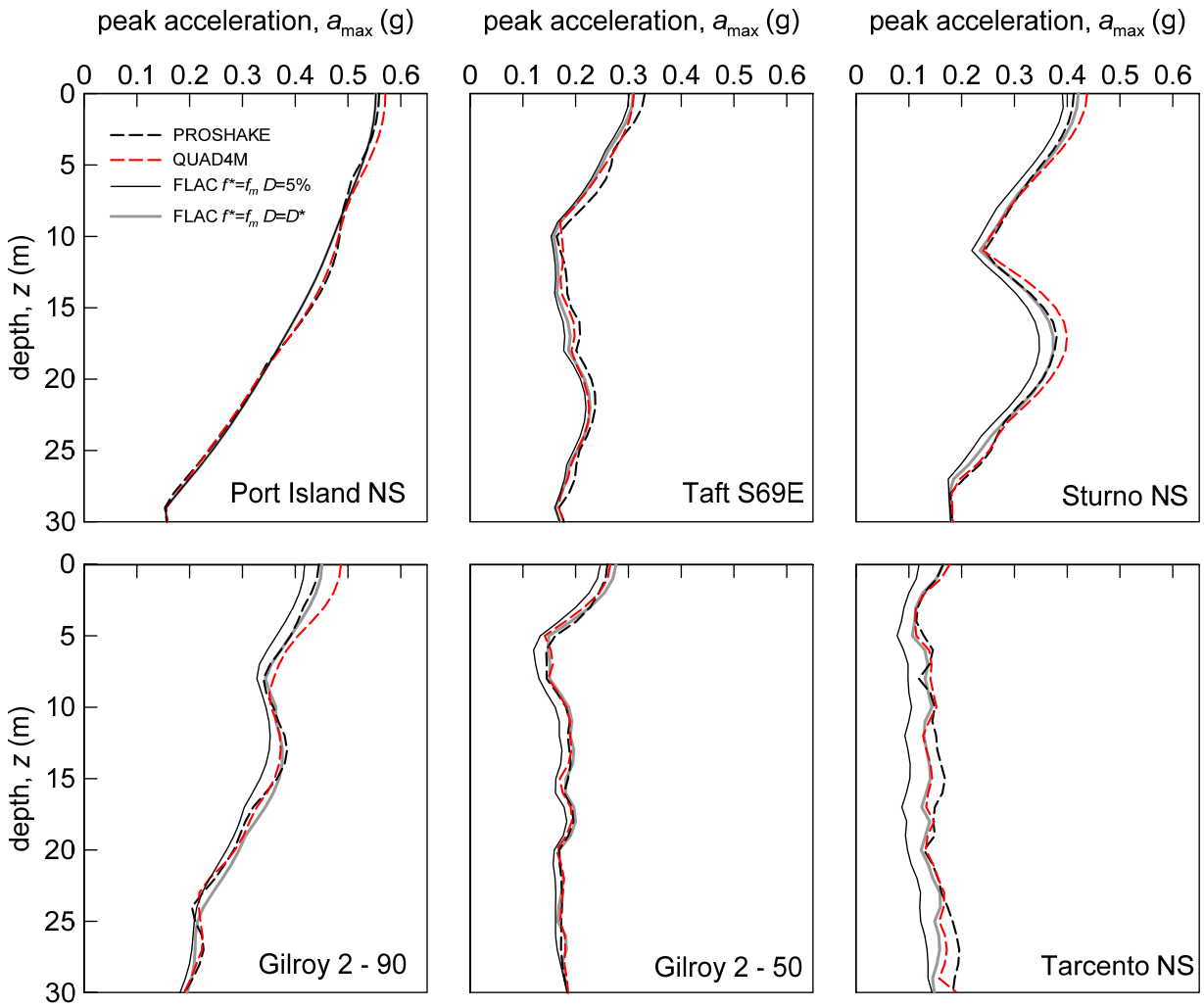

Figure 8. FLAC single control frequency Rayleigh formulation: comparison of PGA profiles for all selected input accelerograms ($f^*=f_m$ and different D^* values) – V_S=100 m/s homogeneous soil deposit (f_0=0.83 Hz)

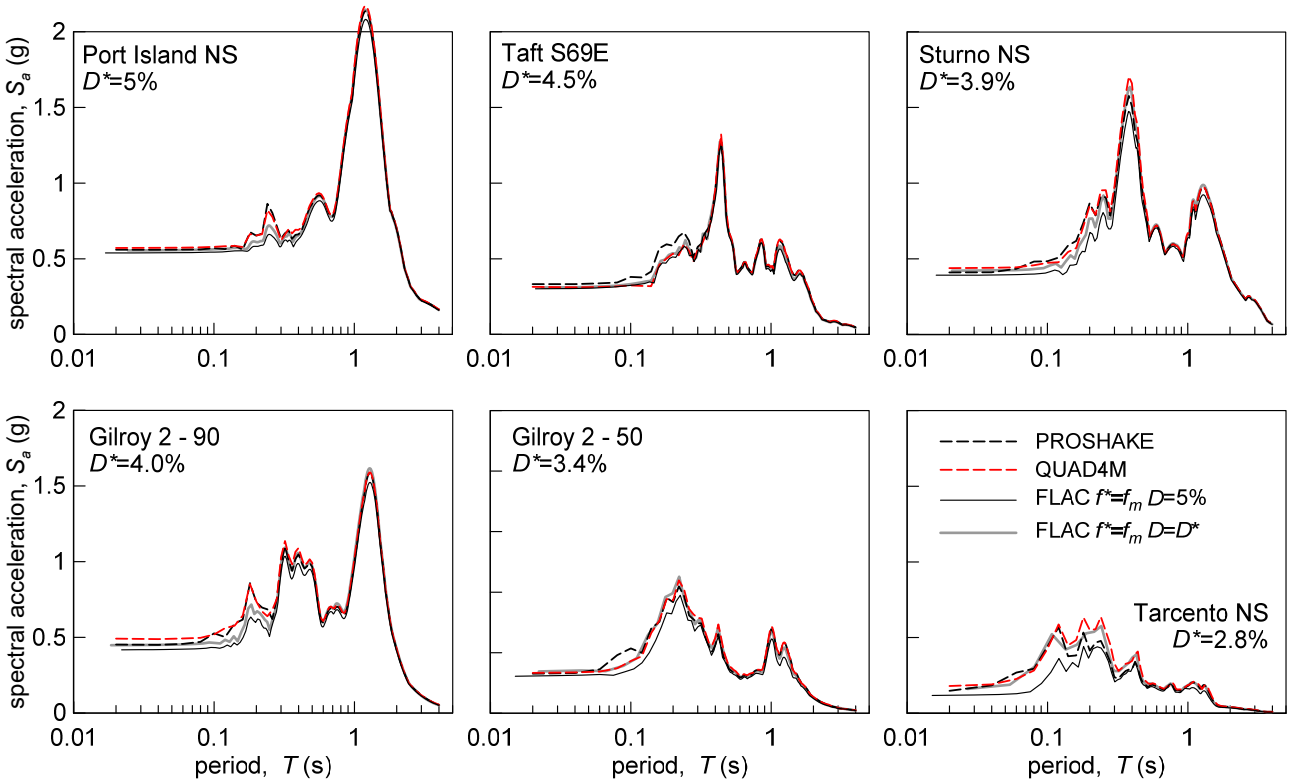

Figure 9. FLAC single control frequency Rayleigh formulation with reduced nominal damping ($f^*=f_m$ and D^*): comparison of response spectra at the surface of soil deposit for all selected input accelerograms – V_S=100 m/s homogeneous soil deposit (f_0=0.83 Hz)

3.3. Comparison between Local/Combined and Rayleigh damping

The second goal of the parametric analyses on the virtual soil deposit has been the quantitative evaluation of the performance of the Local/Combined damping formulations with respect to the "standard" Rayleigh damping, previously presented for a shear wave velocity of V_S=100 m/s.

The frequency independent LD and CD formulations were employed by using D=5% to compute the coefficient α (see Equation (15)). The results in terms of PGA profiles and response spectra at soil surface are compared with Rayleigh results (using f_m and D^*) in Figures 10 and 11 respectively for the six input motions. The comparison clearly highlights the overestimation of the response at medium-to-high frequencies by Local/Combined formulations with respect to Rayleigh analyses; this behavior is particularly pronounced per $T < 0.2$ s and for the LD formulation. On the contrary at longer periods Local/Combined

spectral accelerations satisfactorily match the values predicted by Rayleigh formulation. The overestimation at medium-to-high frequencies greatly affects the peak accelerations thus resulting in Local/Combined PGA profile shifted on the right with respect to Rayleigh analyses (Fig. 10). The PGA overestimation along the profile with respect to the Rayleigh solution is on average 20% and 60% for CD and LD formulations, respectively. The Combined formulation therefore gives results more comparable with the reference as also testified by the lower values of RSS (assuming Rayleigh as reference) with respect to Local damping reported in Table 5. Finally, the Table 6 summarizes the numerical timestep durations pertaining to the analyses carried out with the different FLAC damping formulations. Timestep in Local/Combined analyses (which is the same) is on average a factor 10 higher than in Rayleigh analyses which in turns leads to 10 times faster analyses. The analyses therefore showed that in the face of an overestimation of the high frequencies (limited within 20% for CD), the frequency-independent formulations have an undoubted benefit in terms of significantly faster analysis times.

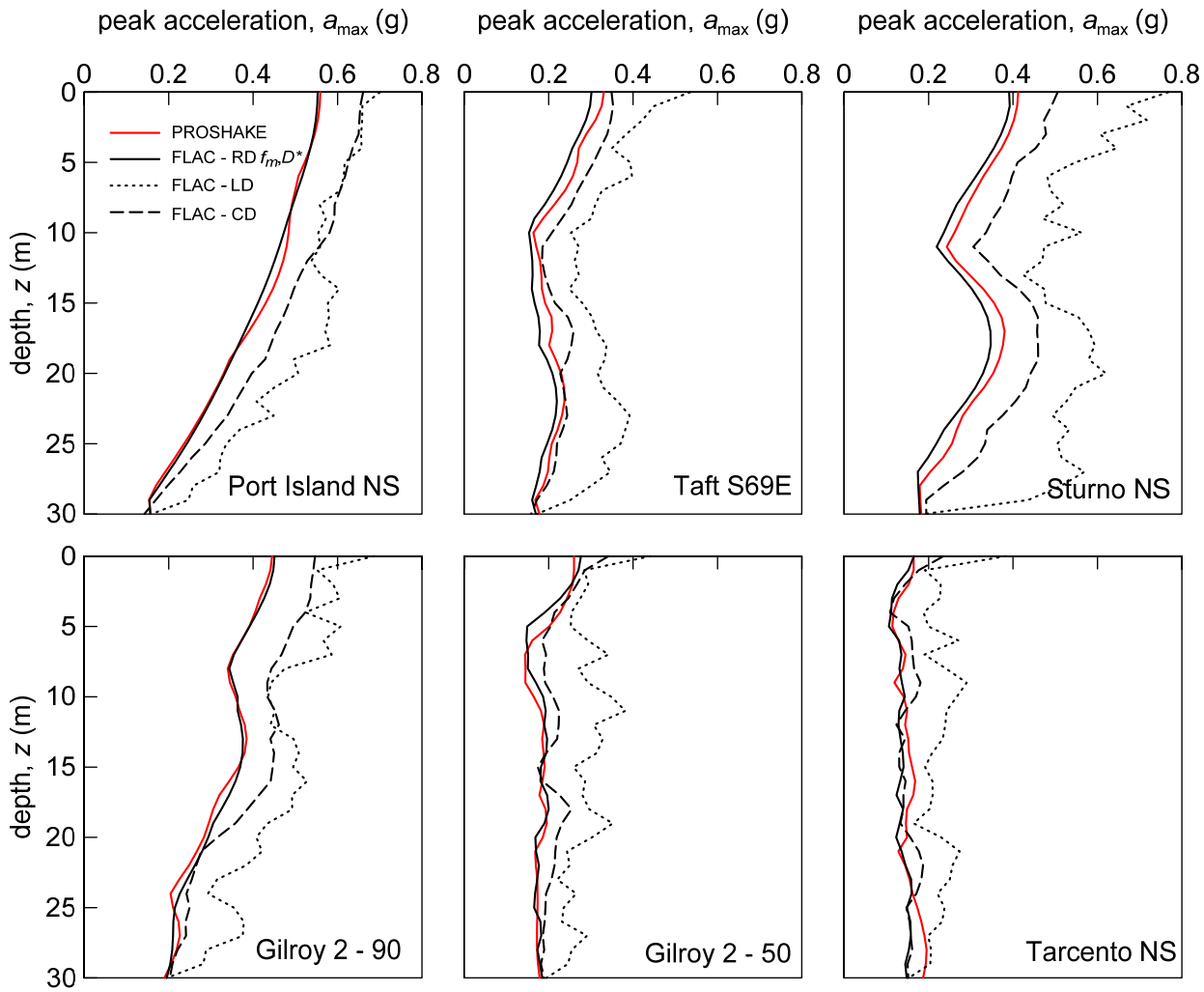

Figure 10. Comparison of PGA profiles for all selected input accelerograms (Rayleigh, local and combined formulations) – V_S=100 m/s homogeneous soil deposit (f_0=0.83 Hz)

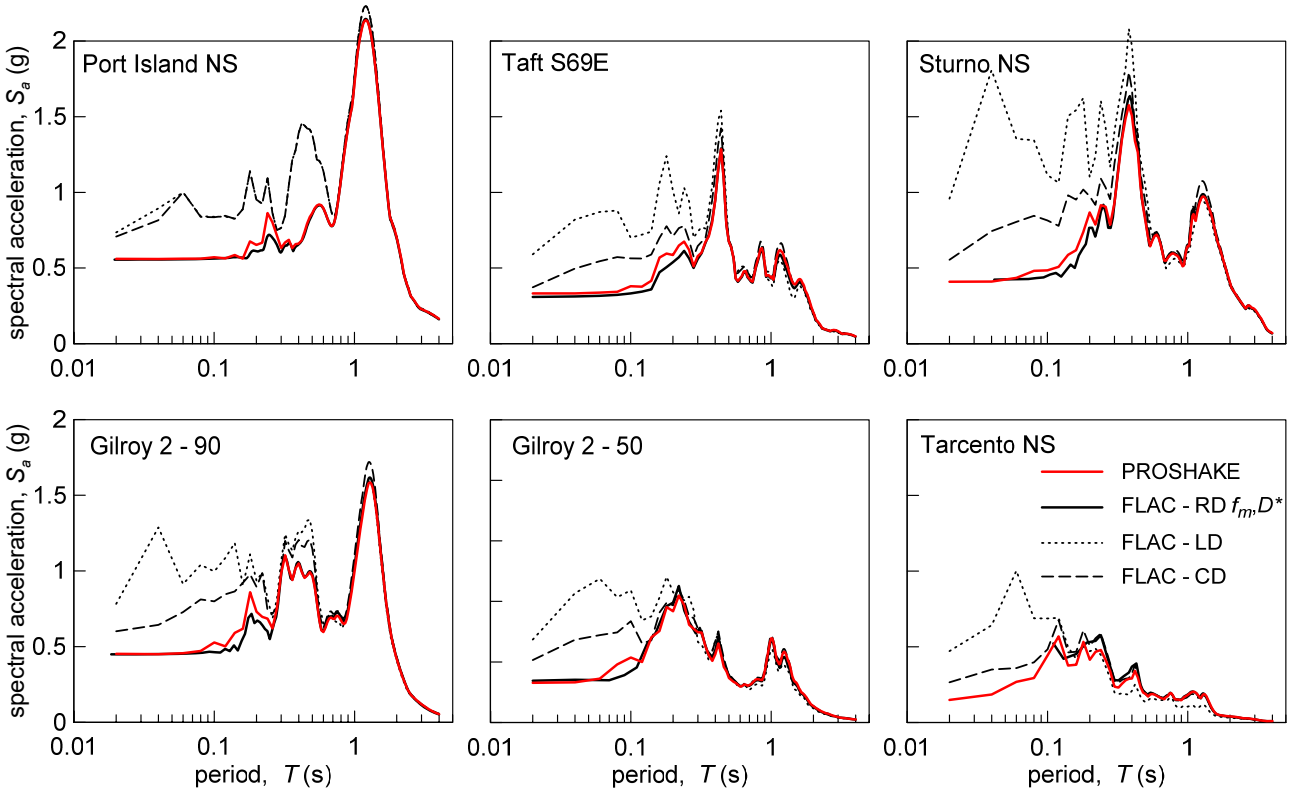

Figure 11. Comparison of response spectra at soil deposit surface for all selected input accelerograms (Rayleigh, local and combined formulations) – V_S=100 m/s homogeneous soil deposit (f_0=0.83 Hz)

Table 5. RSS values computed for FLAC analyses to evaluate the performance of Local/Combined damping formulations with respect to single control frequency Rayleigh formulation (f*=fm and D= D*)

		#1	#2	#3	#4	#5	#6
RSS from PGA Profile	local damping	6.11	3.56	10.68	3.82	1.80	1.76
	combined damping	2.17	0.91	2.56	1.91	0.57	0.70
RSS from Response Spectra	local damping	0.50	0.52	1.78	0.60	0.37	0.30
	combined damping	0.19	0.05	0.20	0.16	0.032	0.02

Table 6. Comparison of time step durations for FLAC analyses carried out with Rayleigh and Local-Combined damping formulations

	#1	#2	#3	#4	#5	#6
Rayleigh Damping	7.55E-06	2.30E-05	2.07E-05	1.81E-05	4.31E-05	5.23E-05
Local-Combined Damping	1.89E-04	1.89E-04	1.89E-04	1.89E-04	1.89E-04	1.89E-04
duration ratio (LD&CD/RD)	9.95	16.18	18.11	20.52	8.56	7.02

4. FLAC seismic analyses of a concrete gravity dam

Licodia Eubea dam is a 65-m-high concrete gravity dam located in South-eastern Sicily (Southern Italy). This area is one of the most seismically active areas of Italy; seismotectonic

studies highlights that two tectonic features are the most critical for the seismic hazard at the site with maximum magnitude estimated to be 6.4 and 6.8 and distance 13 and 5 km, respectively. 7 natural accelerograms were selected as input and scaled such that their average horizontal spectrum (critical damping ratio 5%) reasonably matched the target response spectrum, i.e. the NTC08 National code spectrum on rigid horizontal outcrop having a return period of 1460 years (Collapse Limit State with a residual probability of 5% over a reference period of 75 years).

Figure 12 shows the numerical model of the tallest monolith of the dam subjected to a maximum operating level of the reservoir (328 m a.s.l.). The dam is founded on calcareous sound rock layers intercalated with marly-clayey layers. Structural and geotechnical campaigns included extensive in situ investigations and laboratory testing on concrete and foundation materials (Lanzo *et al.*, 2017). Selected cores of concrete and foundation material were tested to determine physical and mechanical properties of interest; geophysical tests were also conducted both within the dam body and at the bedrock to obtain shear and compressional wave velocities. The physical and mechanical properties adopted in the modelling are summarized in Table 7. The dam body was divided into two zones, an upper one extending approximately from the crest to the mid height and a lower one going down to the bottom of the dam, this latter part being slightly stiffer than the former as resulted from the dam body surveys. Analogously, for the foundation rock two layers have been considered, i.e. a deeper rock mass stiffer than the superficial one, the latter being affected by an higher degree of jointing at lower confining stress. The surficial rock mass immediately below the foundation was assumed as stiff as the deep rock layer due to grouting interventions carried out before the dam body construction. The recent lacustrine infilling at the reservoir bottom, consisting of silty-clayey soils, have been characterized by assigning physical and mechanical values from literature studies.

Table 7. Material properties assumed for dynamic analyses of Licodia Eubea concrete dam

Material		γ (kN/m^3)	V_S (m/s)	V_P (m/s)	E_{dyn} (GPa)	ν (-)	D (%)	D^*(%)
dam	upper zone	23.4	2020	3800	25.6	0.30	8.0	8.5
	lower zone		2140	4000	28.4			
foundation	shallow not consolidated layer	23.0	600	1500	2.4	0.40	1.0	1.1
	deep layer/consolidated zone		900	2200	5.3		0.5	0.53
infilling sediments		15.7	150	1440	0.1	0.495	2.5	2.6

The values of D* are computed according to Equation (19) using f_0= 3 Hz as fundamental frequency of the foundation-dam-sediment-reservoir system and f_m=2.7 Hz as mean frequency of Vasquez Rocks P input motion adopted for the analysis

The numerical procedure developed in two steps: 1) initial static analysis of the dam-foundation rock system; 2) linear dynamic analysis of the dam-water-sediments-foundation rock system (Verrucci *et al.*, 2017).

The static analysis (step 1) aimed at computing the response of the dam-foundation rock system to both the self-weight of the dam and the hydrostatic forces. Static linear elastic properties have been selected, within the range of values obtained from test results. To this aim a calibration was carried out through matching the computed displacements to the displacements measured during the variations of the water levels in the reservoir.

For the dynamic analyses (step 2), viscous dashpots are placed at the bottom boundary in order to take into account radiation damping. "Free-field" conditions are ensured at the two lateral boundaries thus reproducing the 1-D type of motion produced far from the dam by in–plane vertically incident SV waves on horizontally stratified half-space (Fig. 12). A linear elastic medium was assumed for both the body of the dam and the foundation rock. All the amount of material damping is therefore modelled using either Rayleigh or Local/Combined damping formulations without introducing hysteretic damping due to the nonlinear behavior to model. This is a standard choice in dynamic analysis of concrete dams at least in a first verification phase and it is justified by the high stiffness of concrete. Further nonlinear analyses are usually scheduled only if some performance parameters are not reached in the first linear ones. For the purposes of the present paper the linear analyses allow to better highlight the differences between the damping formulations.

A perfect adhesion at concrete-rock interface was considered. Interface elements simulated the dam-water and the foundation-water contacts; these elements are characterized by null shear resistance and normal tensile strength equal to cavitation threshold. The water of the reservoir was treated as a compressible fluid (bulk modulus K=2·10^9 Pa), with a negligible shear modulus, producing hydrodynamic pressures that are dependent on the excitation frequency. Damping ratio (D) assumed for concrete is 8%, which is in the range suggested for dynamic analyses of dams for high seismic loadings (USACE, 1999). For surficial and deep/consolidated rock the damping ratio was assumed equal to 1.0% and 0.5% respectively.

The three different formulations here studied were adopted to model damping properties for the dam body, the bedrock and the reservoir bottom infilling: 1) Rayleigh damping using D^* computed for each material through Equation (19) and assuming f_0= 3 Hz as fundamental frequency of the foundation-dam-sediment-reservoir system (Verrucci *et al.*, 2017), 2) Local and 3) Combined damping, both with coefficient α computed using Equation (15) and D=8% for dam, 0.5-1% for foundation rock and 2.5% for sediments. The values of D^* assumed for Rayleigh damping analyses are also reported in Table 7.

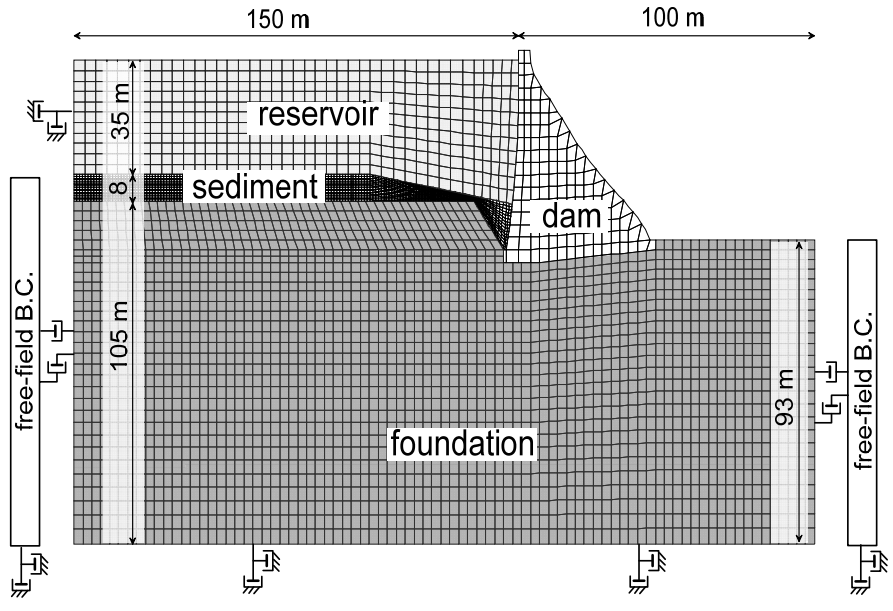

Figure 12. Numerical model of the dam-reservoir-sediment-foundation system for Licodia Eubea concrete gravity dam.

Spectral acceleration values computed at the outcrop (point O) and at typical zones of the dam (crest, C; upstream and downstream toes T1 and T2) are represented in Figure 13. Among the 7 signals employed in the analyses results are shown for the input acceleration time history for which most critical results has been obtained (Vasquez Rocks P station, Northridge 1994 earthquake, component NS, scaled by 3.5, f_m=2.7 Hz and f_p=5 Hz, Lanzo *et al.*, 2017). The different damping formulations predict a very similar response at the downstream rock outcrop that is justified by the very low damping ratios adopted for the foundation rock mass (0.5 - 1.0%). High discrepancies can be observed on the dam body, especially for the LD formulations that significantly overestimates the accelerations in the medium-to-high frequency range ($T < 0.2$ s) in agreement with the numerical results obtained on the ideal soil deposit. On the contrary the CD provides a more satisfactory performance being spectral accelerations closer to the RD results. The numerical overestimation of the high frequencies can be significantly reduced through calculating the mean of the acceleration time histories of close nodes adjacent to the same zone of the finite difference mesh. The results obtained through this elaboration are shown with the red point lines in Figure 13 for the LD formulation only. The CD results obtained with the same procedure are not reported because they are practically coincident to the RD spectra.

An analogous effect can be observed in terms of horizontal relative crest-toe displacements (Figure 14a). The elastic displacement oscillations (less than 2 cm wide) develop without significant differences between the different damping formulations and the Fourier amplitudes show that the high frequency overestimation observed in the punctual acceleration time-histories is almost disappeared in the relative displacement time histories (Fig. 14b). The effect is drastic for the combined damping analysis but it is also significant for the local damping one.

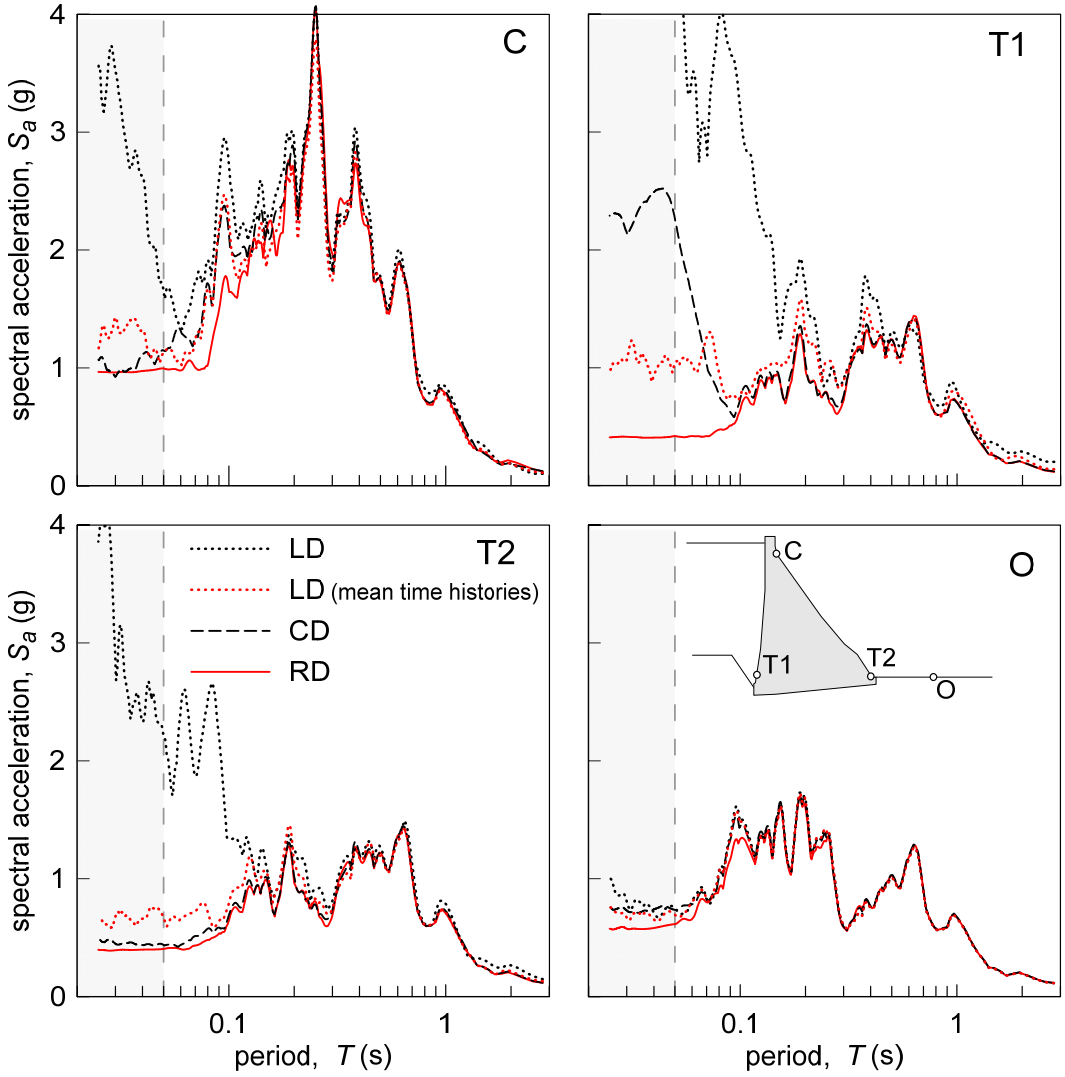

Figure 13. Acceleration response spectra computed in typical points according to the three different damping formulations.

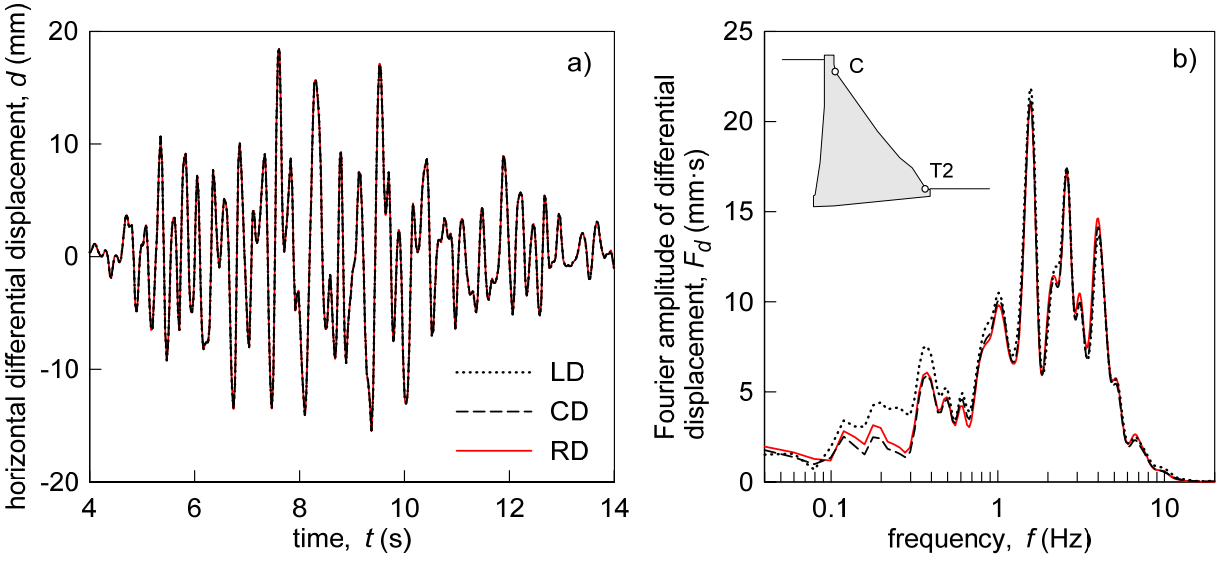

Figure 14. Relative crest-toe displacement compute according to the three different damping formulations.

Figure 15 shows the contour lines of the maximum temporal value (upper envelope) of the principal tensile stress reached in the dam body. Separate plots are reported for the three different damping formulations adopted in the analysis.

The qualitative pattern of the local maximum tensile stresses is quite similar for the different damping formulations: the plots confirm that higher tensile stresses develop at the heel and at the toe of the dam as well as near the changes of slopes of upstream and downstream faces. The largest values occur at the heel of the dam, where the allowable tensile strength (f_t =1.25 MPa based in available data) is exceeded only in localized areas. Figure 16 shows the time histories of the maximum principal stress (either maximum tensile stress or minimum compressive stress) computed at two representative zones located at the heel (point H) and at the downstream face (point P) in the strongest time interval of the earthquake. The oscillations of the tensile stress are very similar among the three damping formulations and minor differences can be observed only in correspondence of the peaks. The peaks are reached alternatively in the heel and in the downstream zones, thus reflecting the global oscillation of the dam body characteristic of the first vibration mode. The maximum value of a peak is reached indifferently by one of the three formulations. The absolute maximum value is reached for both the observation points by the LD formulation but with a not significant excess with respect to the second lower peak. This apparent similarity indicates that the irregularities induced by the acceleration discontinuities in the LD and CD formulations are dramatically reduced. In fact strains, then also stresses, arise from the gradient of the displacement field whose time histories are noticeably smoothed with respect to the acceleration ones (see Appendix A).

The amplitude differences between the stress histories can be effectively not negligible, in particular around the peaks. Nevertheless these should be considered preliminary analyses with the aim of assessing the effective need of further non-linear analyses. Therefore the performance should be judged on the base of global evaluations. For the seismic

performance assessment and damage estimation, some performance indices proposed by the USACE guidelines (2007) can be employed. In this approach, once defined a “local” index as the stress demand-capacity ratio DCR (i.e., the ratio between the calculated maximum tensile stress in a point and the tensile strength of the concrete), a global performance test is shown in Figure 17. It represents the fractions of the dam body section over which an increasing demand-capacity ratio is reached (i.e. the area on which the tensile strength is exceeded with a DCR increasing from 1 to 2). In this context a nearly indistinguishable performances obtained through RD e CD formulations is verified, while the LD formulation is slightly disadvantageous, exceeding at DCR=2 the limit state represented by the red line (USACE, 2007). More details on dam performance can be found in Lanzo *et al.*, (2017) which reports also more advanced nonlinear analyses showing an acceptable margin of safety of the dam under the selected CLS scenario.

In conclusion, the use of combined damping formulation allowed to perform an accurate estimation of the seismic performance of the concrete dam, taking advance with respect to the Rayleigh damping analyses of an increased time step length. In the blow-up window of Figure 16, values at each effective time step are marked for both the LD and CD formulations, while only one value every five time steps are marked for the RD formulation. Time step in the analysis of both LD and CD formulations (3.0E-3), is long about 150 times the time step in the RD formulation (2.2E-5). This means, for the input motion here considered (25 s long), a time analyses of about 40 minutes instead of 3 days for a calculator equipped with a 2.50 GHz CPU processor, RAM 16 GB.

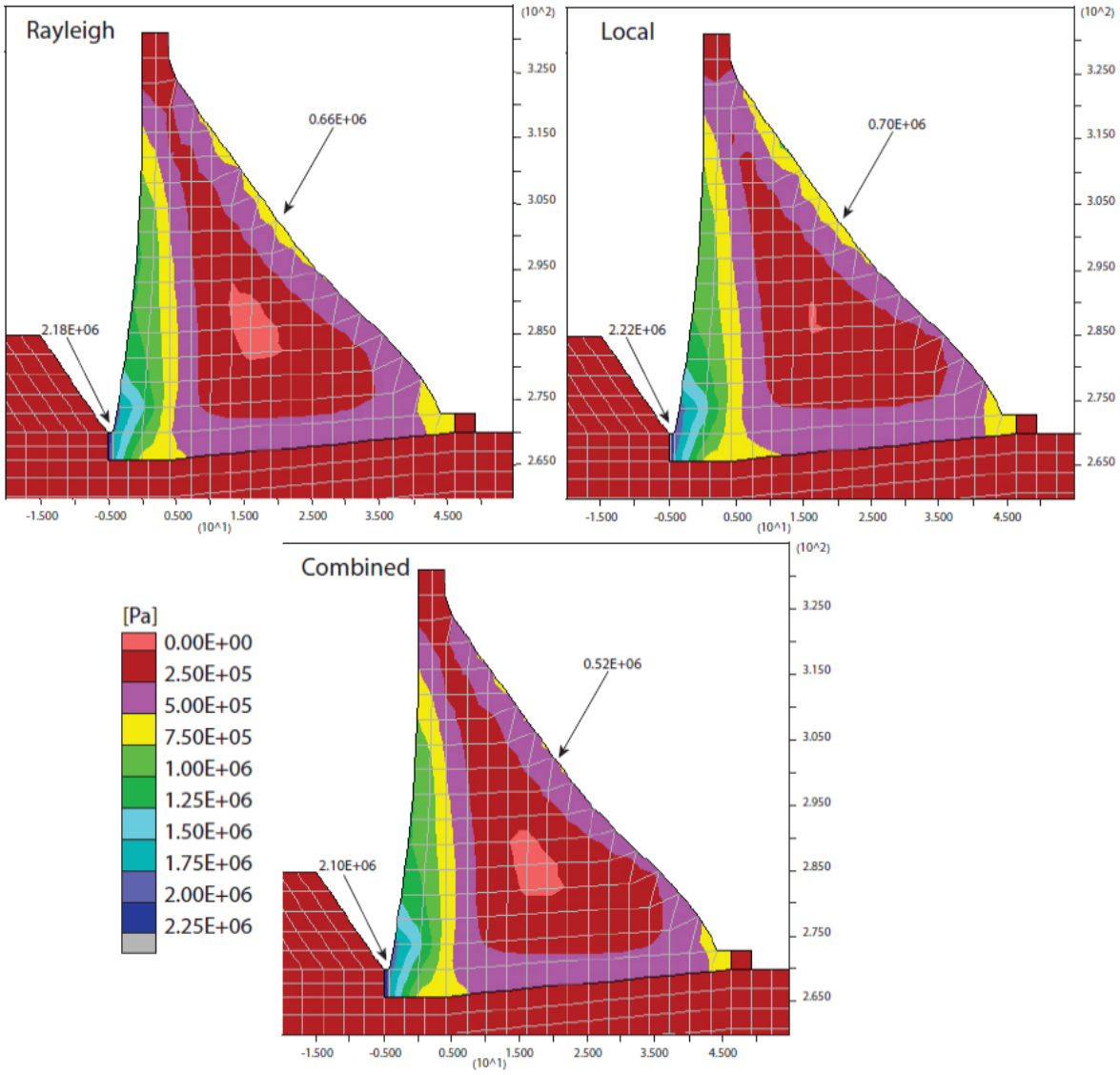

Figure 15. Contours of principal tensile stress envelopes in the dam body for the 3 damping models (most severe input motion) – stresses are expressed in Pa

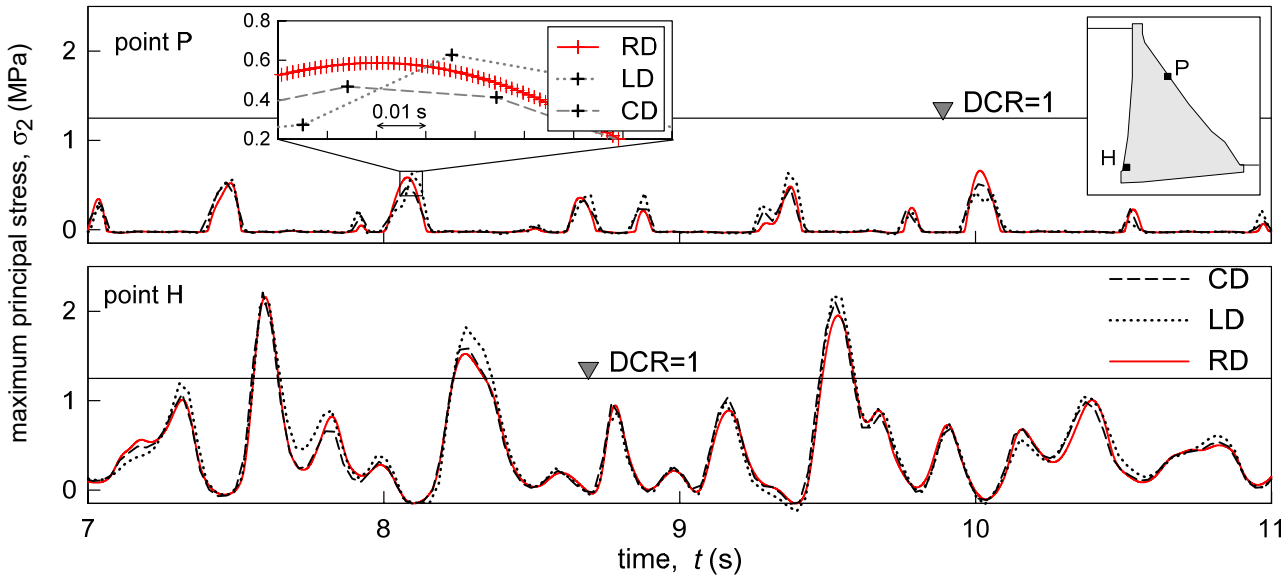

Figure 16. Time histories of the principal tensile stress computed at two representative elements of the dam body for the three adopted damping formulations

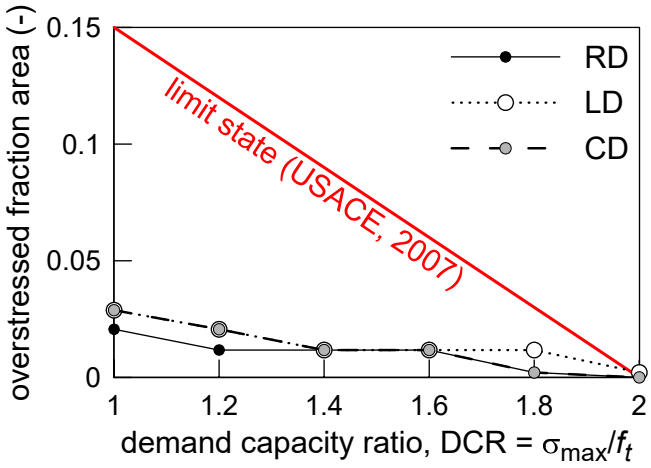

Figure 17. Fraction areas of the dam body section that area stressed over the tensile strength vs. the demand capacity ratio.

5. Conclusions

The performance of the different damping formulations implemented in FLAC code, namely Rayleigh, Local and Combined, has been analysed in the paper. These formulations are generally adopted to model either the full damping properties of materials in linear analyses or the small-strain damping in elastoplastic and hyperbolic (hysteretic) nonlinear analyses. The focus was addressed to the linear analyses that are adequate to assess the dynamic

behaviour of a system for low to medium strain levels and that are also used as preliminary analyses to assess the necessity of further nonlinear ones.

After a theoretical background of the different formulations in the finite difference code FLAC, linear dynamic analyses on ideal homogeneous soil deposits excited by different accelerograms are presented. As a first check, by setting a soil damping of 5%, the PGAs profiles and response spectra obtained using Rayleigh damping with different single control frequencies f^* were compared with results from a frequency domain code assumed as reference (frequency-independent damping solution). These analyses highlight that for input characterized by mean frequency $f_m < f_0$ (fundamental frequency of deposit) no appreciable influence of f^* selection is observed; a simple $f^*=f_0$ can be recommended. On the contrary for input characterized by f_m above f_0, the use of target D and f^* values producing the same damping-frequency curve of the two-control frequencies QUAD4M approach (D_{min} and f_{min}) allows to minimize the differences with the reference to the frequency-independent damping solution. Further analyses have been carried out by using $f^*=f_m$ and varying the target damping D^*. An expression for the evaluation of D^* to minimize the overdamping of the highest frequency is proposed for practical use. The results of the analyses show that Rayleigh formulation with f_m and proposed D^* give results in a satisfactory agreement with the frequency-independent damping solution and sometimes even better than the f_{min}-D_{min} approach. Subsequently, a series of analyses have been performed using Local and Combined damping frequency-independent formulations implemented on FLAC, comparing them with the best Rayleigh formulation (f_m, D^*) assumed as reference. The analyses have shown that both Local/Combined formulations introduce noises at high frequencies, but significantly reduce calculation times by a factor of 7 to 20. Between the two formulations, the Combined formulation seems more reliable with an average overestimation of about 20% in terms of PGA.

Finally, 2D dynamic analyses were conducted on the seismic response of a concrete gravity dam. A linear model has been assumed and therefore all dissipative properties of the concrete dam were modelled through Rayleigh/Local/Combined damping to focus on the differences among the different formulations. The comparison has been presented in terms of response spectra, displacements, tensile stress time histories at selected points and contours of envelopes of principal tensile stresses in the dam body. The results show that Combined damping formulation satisfactorily approximates the results of the more rigorous Rayleigh damping formulation. Dynamic analyses with Rayleigh method carried out with a typical personal computer (2.50 GHz CPU processor, RAM 16.0 GB) need 60-70 hours for each accelerogram of the input suite of signals while the Local/Combined analyses only require 20-40 minutes of running.

As a conclusion all the comparative analyses prove that the frequency-independent LD and CD formulations provide significantly faster running times in dynamic analyses with respect to the “standard” Rayleigh formulation but produce an overestimation of the spectral acceleration at high frequencies as drawback. The CD formulation is effective in reducing significantly this overestimation, providing results that in general stay between those of the LD and RD formulations. The overestimation can be further diminished if an averaging procedure is applied on the time histories of a set of adjacent nodes (for example the nodes at the vertexes of a single zone). Furthermore the strain and stress histories are much less disturbed than the acceleration histories because they are calculated from the displacement histories, weakly influenced from the discontinuities of acceleration time histories. Therefore the seismic performance in term of strain-stress is practically coincident to that obtained by the Rayleigh formulation especially for the those systems that are primarily governed by the low frequency vibration modes.

The seismic behaviour of the analyzed systems is clearly captured by the Combined damping (CD) formulation which is therefore suitable for time consuming sensitivity analyses

in the first phases of a study or for projects whose running times should be limited to acceptable values (3D models, large 2D models, soil-foundation-structure dynamic interaction analyses among others). However the users should be aware of the limitations associated with the combined damping which may have discrepancies of acceleration spectrum at high frequencies against the results by the reference Rayleigh damping.

ACKNOWLEDGMENTS

The work presented in this paper was partly supported by the financial contribution of the Italian Department of Civil Protection within the framework “RELUIS-DPC” which is greatly acknowledged by the authors. The Authors are grateful to “ENI - Raffineria di Gela” for permitting the publication of data about the dam. The anonymous reviewers are acknowledged for their precious comments and suggestions on the manuscript.

REFERENCES

Bathe, K. J., and E. L.Wilson (1976). Numerical Methods in Finite Element Analysis. Englewood Cliffs, New Jersey: Prentice-Hall Inc. (1976).

Chopra A.K., (2007). Dynamics of structures. Pearson Prentice Hall. Upper Saddle River, New Jersey.

Cundall PA. (2006) *A simple hysteretic damping formulation for dynamic continuum simulations*. In: de Varona P, Hart RD, editors. FLAC and numerical modeling in geomechanics 2006. Proceedings of the 4th international FLAC symposium, 2006. Madrid (Spain): Itasca Consulting Group; 2006.

Dawson E.M., Cheng Z. (2021). *Maxwell damping: an alternative to Rayleigh damping*. Geo-Extreme 2021: Infrastructure Resilience, Big Data, and Risk. Meehan C.L., Pando M.A., Leshchinsky B.A., Jafari N.H. Eds.. ISBN (PDF): 9780784483701. https://doi.org/10.1061/9780784483701.004.

EduPro Civil System, Inc. (1998). ProShake – Ground Response Analysis Program. EduPro Civil System, Inc., Redmond, Washington.

Hashash Y. M. A., Park D. (2001). Non-linear one-dimensional seismic ground motion propagation in the Mississippi embayment. Engineering Geology, 62, 18-206.

Hudson M, Idriss I, Beikae M (1994) User's manual for QUAD4 M. Center for Geotechnical Modeling, Department of Civil and Environmental Engineering, University of California, Davis, California

Itasca (2011). FLAC-Fast Lagrangian Analysis of Continua, Ver. 7.0. User's Guide. Itasca Cons. Group, Minneapolis, USA.

Joyner W.B., Chen A.T.F. (1975). Calculation of nonlinear ground response in earthquakes. Bulletin of Seismol. Society of America, 65(5), 1315-1336 (1975).

Kwok A. O., Stewart J. P., Hashash Y. M., Matasovic N., Pyke R., Wang Z., Yang Z. (2007). Use of exact solutions of wave propagation problems to guide implementation of nonlinear seismic ground response analysis procedures. Journal of Geotechnical and Geoenvironmental Engineer 133(11). ©ASCE, ISSN 1090-0241/2007/11-1385–1398/$25.00, https://doi.org/10.1061/(ASCE)1090-0241(2007)133:11(1385)

Lanzo G., Pagliaroli A., D'Elia B. (2003). Numerical study on the frequency-dependent viscous damping in dynamic response analyses of ground. In: Earthquake Resistant Engineering Structures IV edited by Latini & Brebbia, WIT Press, Southampton, Boston, pp. 315-324.

Lanzo G., Pagliaroli A., D'Elia B. (2004). Influenza della modellazione di Rayleigh dello smorzamento viscoso nelle analisi di risposta locale. Atti del XI Convegno Nazionale "L'Ingegneria Sismica in Italia", ANIDIS, Genova, 25-29 gennaio 2004, Servizi Grafici Editoriali, Padova, CD-ROM, paper #A1-02. ISBN: 88-86281-89-7.

Lanzo G., Verrucci L., Pagliaroli A., Scasserra G. (2017). Seismic safety assessment of a concrete gravity dam in Southeastern Sicily. Atti XXVI Convegno Nazionale di Geotecnica, 20-22 Giugno, Roma, vol. 2, pag. 1087-1095. ISBN: 978-88-97517-09-2

Liu Y, Li H, Xiao K, Li J, Xia X, Liu B. (2014). Seismic stability analysis of a layered rock slope. Comput Geotechnics 55, 474–81.

Lysmer J., Kuhlemeyer R.L. (1969). Finite Dynamic Model for Infinite Media. J. Eng. Mech., 95(EM4), 859-877.

Manica M., Ovando E., Botero E. (2014). Assessment of damping models in FLAC. Computers and Geotechnics 59 (2014) 12–20.

Masing, G. (1926). “Eigenspannungen undVerfertigung beim Messing,” in Proceedings, 2nd International Congress on Applied Mechanics. Zurich, Switzerland.

Matasovic, N. (2006). D-MOD_2—A computer program for seismic response analysis of horizontally layered soil deposits, earthfill dams, and solid waste landfills, user’s manual, GeoMotions, LLC, Lacey, Wash., 20 p.

Park D., Hashash Y. M. A. (2004). Soil damping formulation in nonlinear time domain site response analyses. Journal of Earthquake Engineering, Vol. 8, No. 2 (2004) 249-274.

Rathje E.M., Abrahamson N., Bray J.D. (1998). Simplified Frequency Content Estimates of Earthquake Ground Motions. Journal of Geotechnical Engineering, 124(2), 150-159.

USACE (1999). Engineering and Design Response Spectra and Seismic Analysis for Concrete Hydraulic Structures. Department of the Army U.S. Army Corps of Engineers Washington, DC 20314-1000 CECW-ET. Engineer Manual 1110-2-6050, 30 June 1999.

USACE (2007). Earthquake Design and Evaluation of Concrete Hydraulic Structures. EM 1110-2-6053.

Verrucci L., Lanzo G., Pagliaroli A., Scasserra G. (2017). The use of FLAC for the seismic evaluation of a concrete gravity dam including dam-water-sediments-foundation rock interaction. Proc. 14th ICOLD International Benchmark Workshop on Numerical Analysis of Dams, Stockholm (Sweden), September 6-8, 2017, 10 pp.

Zienkiewicz, O., C., Taylor R.L. and Zhu J.Z. (2005). The Finite Element Method: Its Basis and Fundamentals. Elsevier Butterworth-Heinemann Oxford.

Appendix A

Relation between local damping coefficient α and material critical damping ratio D

The harmonic motion of a linear single degree of freedom system with undamped natural circular frequency ω_0 is characterized by the following time histories of displacement, u, velocity, $\dot{u}$ and elastic force, F (Fig. A1):

$$u(t) = A\sin(\omega_0 t) \quad (A.1)$$

$$\dot{u}(t) = A\omega\, cos(\omega_0 t) \quad (A.2)$$

$$F(t) = -ku = -kA\sin(\omega_0 t) \quad (A.3)$$

A and *k* being the displacement amplitude and the elastic constant respectively. If a local damping is applied as in (15) using a coefficient α <1 the damping force is:

$$F_d = -\alpha|F|sgn(\dot{u}) = -\alpha k|u|sgn(\dot{u}) \quad (A.4)$$

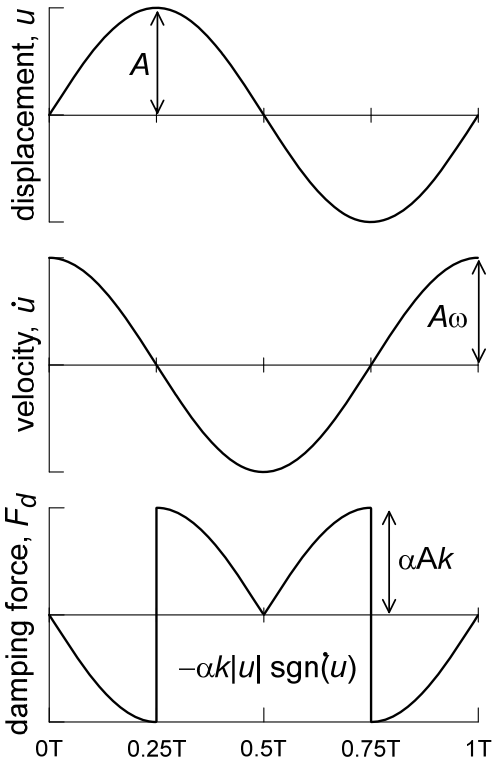

Figure A1. Motion of a free linear elastic single degree of freedom system and the associated damping force in the LD formulation

The equilibrium is:

$$F + F_d = m\ddot{u} \quad (A.5)$$

that can be expressed as:

$$\frac{m}{1 \pm \alpha}\ddot{u} + ku = 0 \quad (A.6)$$

the higher and lower signs in the acceleration coefficient are valid when the damping force is negative (first and last quarters of each cycle) and positive (central quarters of each cycle)

respectively. It is apparent that the Equation (A6) is that of an undamped system having a mass modified by the factor $1/(1\pm\alpha)$ and a modified circular frequency ω_α:

$$\omega_\alpha = \sqrt{\frac{k(1 \pm \alpha)}{m}} \quad (A.7)$$

For example, the motion of a free single degree of freedom system damped through the local damping formulation is shown in Fig A2. The input parameters are mass m= 1 kg, natural undamped period T_0= 1.2 s, critical damping ratio D= 10%, initial velocity v_0= 1 m/s. The motion of a traditional viscous damped system with the same parameters is shown through the gray dotted lines. In Figure A3 the time histories of both the elastic force and the damping force are shown.

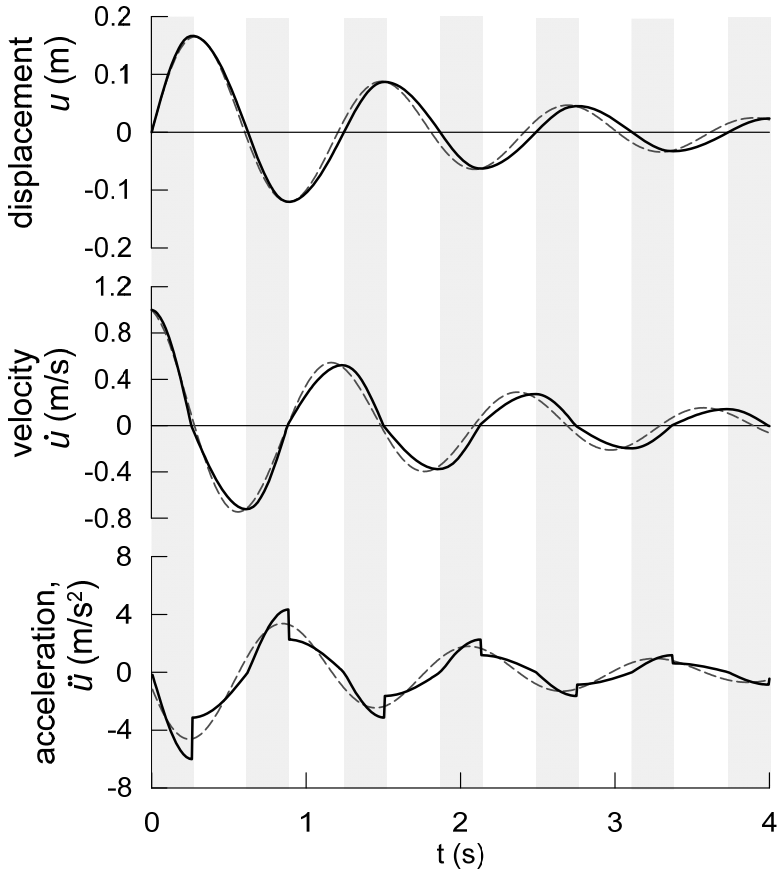

Figure A2. Free motion of a linear elastic single degree of freedom system damped through the LD formulation (critical damping ratio, D=10%) in terms of displacement u, velocity $\dot{u}$ and acceleration $\ddot{u}$. Dotted lines represent the response of a viscously damped system with same damping ratio. Grey and white coloured areas indicate time ranges for which the LD formulation is equivalent to a free motion with a mass diminished or increased, respectively.

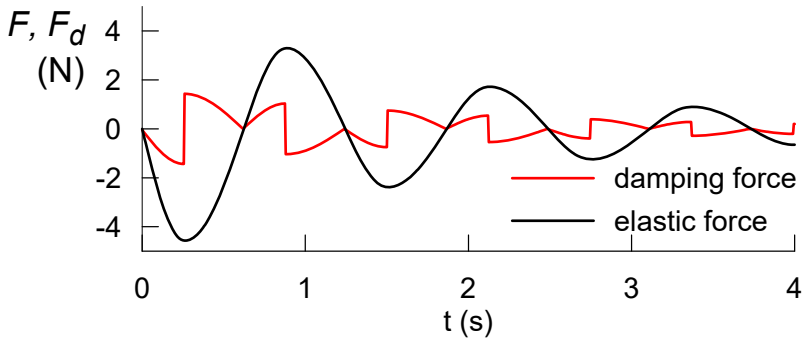

Figure A3 Damping force and elastic force of the single degree of freedom system damped through the LD formulation (*D*=10%).

The damping force is always opposite respect to the velocity and the energy dissipated during each quarter of the period T_α is constant and can be calculated for the first quarter (when and F_d=-$\alpha k u$) as:

$$\Delta w = -\int_0^{\frac{T_\alpha}{4}} F_d\, \dot{u}\, dt = \int_0^{\frac{T_\alpha}{4}} \alpha k A \sin(\omega_\alpha t)\, A\omega^* \cos(\omega_\alpha t)\, dt = \frac{\alpha k A^2}{2} \quad (A.8)$$

Therefore the work dissipated in the whole cycle:

$$\Delta W = 4\Delta w = 2\alpha k A^2 \quad (A.9)$$

The maximum elastic energy W_E accumulated at the displacement peak u_{max} is:

$$W_E = \frac{1}{2} u_{max} F_{max} = \frac{1}{2} k A^2 \quad (A.10)$$

and the critical damping ratio *D* can be calculated:

$$D = \frac{\Delta W}{4\pi W_E} = \frac{\alpha}{\pi} \quad (A.11)$$